EUROPEAN ORGANISATION FOR PARTICLE PHYSICS

CERN-PPE/94-49
17 March 1994

Measurement of the Production Rates of Charged Hadrons in e^+e^- Annihilation at the Z^0

The OPAL Collaboration

Abstract

The inclusive production rates of $\pi^{\pm}$, $K^{\pm}$ and $p\bar{p}$ in Z^0 decays have been measured with the OPAL detector at LEP. Using the energy loss measurement in the jet chamber, the momentum range up to the beam energy (45.6 GeV/c) has been covered. Differential cross sections and total particle yields are given. Comparisons of the inclusive momentum spectra and the total rates with predictions of the JETSET and the HERWIG Monte Carlo model are presented. The total single rates are found to be 17.05 ± 0.43 $\pi^{\pm}$, 2.42 ± 0.13 $K^{\pm}$ and 0.92 ± 0.11 $p\bar{p}$ per hadronic event. Predictions of JETSET for cross sections and total rates agree very well for $\pi^{\pm}$; however, for momenta greater than 4 GeV/c, $K^{\pm}$ rates are underestimated and $p\bar{p}$ rates are overestimated. Combined with data of other particle species there is evidence that the peak positions in the $\xi = \ln(1/x_p)$ distributions show a different mass dependence for mesons and baryons. However, both JETSET and HERWIG Monte Carlo predictions agree with the observed data.

(Submitted to Zeit. f. Physik)

The OPAL Collaboration

R. Akers[16], G. Alexander[23], J. Allison[16], K.J. Anderson[9], S. Arcelli[2], S. Asai[24], A. Astbury[28], D. Axen[29], G. Azuelos[18,a], A.H. Ball[17], R.J. Barlow[16], S. Barnett[16], R. Bartoldus[3], J.R. Batley[5], G. Beaudoin[18], A. Beck[23], G.A. Beck[13], J. Becker[10], C. Beeston[16], T. Behnke[27], K.W. Bell[20], G. Bella[23], P. Bentkowski[18], P. Berlich[10], S. Bethke[32], O. Biebel[3], I.J. Bloodworth[1], P. Bock[11], B. Boden[3], H.M. Bosch[11], M. Boutemeur[18], P. Bright-Thomas[25], R.M. Brown[20], A. Buijs[8], H.J. Burckhart[8], C. Burgard[27], P. Capiluppi[2], R.K. Carnegie[6], A.A. Carter[13], J.R. Carter[5], C.Y. Chang[17], C. Charlesworth[6], D.G. Charlton[8], S.L. Chu[4], P.E.L. Clarke[15], J.C. Clayton[1], I. Cohen[23], J.E. Conboy[15], M. Cooper[22], M. Coupland[14], M. Cuffiani[2], S. Dado[22], C. Dallapiccola[17], G.M. Dallavalle[2], C. Darling[31], S. De Jong[13], L.A. del Pozo[5], H. Deng[17], M. Dittmar[4], M.S. Dixit[7], E. do Couto e Silva[12], J.E. Duboscq[8], E. Duchovni[26], G. Duckeck[8], I.P. Duerdoth[16], D.J.P. Dumas[6], P.A. Elcombe[5], P.G. Estabrooks[6], E. Etzion[23], H.G. Evans[9], F. Fabbri[2], B. Fabbro[21], M. Fierro[2], M. Fincke-Keeler[28], H.M. Fischer[3], R. Folman[26], D.G. Fong[17], M. Foucher[17], H. Fukui[24], A. Fürtjes[8], A. Gaidot[21], J.W. Gary[4], J. Gascon[18], N.I. Geddes[20], C. Geich-Gimbel[3], S.W. Gensler[9], F.X. Gentit[21], T. Geralis[20], G. Giacomelli[2], P. Giacomelli[4], R. Giacomelli[2], V. Gibson[5], W.R. Gibson[13], J.D. Gillies[20], J. Goldberg[22], D.M. Gingrich[30,a], M.J. Goodrick[5], W. Gorn[4], C. Grandi[2], F.C. Grant[5], J. Hagemann[27], G.G. Hanson[12], M. Hansroul[8], C.K. Hargrove[7], P.F. Harrison[13], J. Hart[8], P.A. Hart[9], P.M. Hattersley[1], M. Hauschild[8], C.M. Hawkes[8], E. Heflin[4], R.J. Hemingway[6], G. Herten[10], R.D. Heuer[8], J.C. Hill[5], S.J. Hillier[8], T. Hilse[10], D.A. Hinshaw[18], P.R. Hobson[25], D. Hochman[26], R.J. Homer[1], A.K. Honma[28,a], R.E. Hughes-Jones[16], R. Humbert[10], P. Igo-Kemenes[11], H. Ihssen[11], D.C. Imrie[25], A. Jawahery[17], P.W. Jeffreys[20], H. Jeremie[18], M. Jimack[1], M. Jones[6], R.W.L. Jones[8], P. Jovanovic[1], C. Jui[4], D. Karlen[6], K. Kawagoe[24], T. Kawamoto[24], R.K. Keeler[28], R.G. Kellogg[17], B.W. Kennedy[15], J. King[13], S. Kluth[5], T. Kobayashi[24], M. Kobel[10], D.S. Koetke[8], T.P. Kokott[3], S. Komamiya[24], R. Kowalewski[8], R. Howard[29], J. von Krogh[11], J. Kroll[9], P. Kyberd[13], G.D. Lafferty[16], H. Lafoux[8], R. Lahmann[17], J. Lauber[8], J.G. Layter[4], P. Leblanc[18], P. Le Du[21], A.M. Lee[31], E. Lefebvre[18], M.H. Lehto[15], D. Lellouch[26], C. Leroy[18], J. Letts[4], L. Levinson[26], Z. Li[12], S.L. Lloyd[13], F.K. Loebinger[16], G.D. Long[17], B. Lorazo[18], M.J. Losty[7], X.C. Lou[8], J. Ludwig[10], A. Luig[10], M. Mannelli[8], S. Marcellini[2], C. Markus[3], A.J. Martin[13], J.P. Martin[18], T. Mashimo[24], P. Mättig[3], U. Maur[3], J. McKenna[29], T.J. McMahon[1], J.R. McNutt[25], F. Meijers[8], F.S. Merritt[9], H. Mes[7], A. Michelini[8], R.P. Middleton[20], G. Mikenberg[26], J. Mildenberger[6], D.J. Miller[15], R. Mir[12], W. Mohr[10], C. Moisan[18], A. Montanari[2], T. Mori[24], M. Morii[24], U. Müller[3], B. Nellen[3], H.H. Nguyen[9], S.W. O'Neale[1], F.G. Oakham[7], F. Odorici[2], H.O. Ogren[12], C.J. Oram[28,a], M.J. Oreglia[9], S. Orito[24], J.P. Pansart[21], P. Paschievici[26], G.N. Patrick[20], M.J. Pearce[1], P. Pfister[10], J.E. Pilcher[9], J. Pinfold[30], D. Pitman[28], D.E. Plane[8], P. Poffenberger[28], B. Poli[2], T.W. Pritchard[13], H. Przysiezniak[18], G. Quast[27], M.W. Redmond[8], D.L. Rees[8], G.E. Richards[16], M. Rison[5], S.A. Robins[13], D. Robinson[5], A. Rollnik[3], J.M. Roney[28], E. Ros[8], S. Rossberg[10], A.M. Rossi[2], M. Rosvick[28], P. Routenburg[30], K. Runge[10], O. Runolfsson[8], D.R. Rust[12], M. Sasaki[24], C. Sbarra[2], A.D. Schaile[26], O. Schaile[10], F. Scharf[3], P. Scharff-Hansen[8], P. Schenk[4], B. Schmitt[3], H. von der Schmitt[11], M. Schröder[12], H.C. Schultz-Coulon[10], P. Schütz[3], M. Schulz[8], C. Schwick[27], J. Schwiening[3], W.G. Scott[20], M. Settles[12], T.G. Shears[5], B.C. Shen[4], C.H. Shepherd-Themistocleous[7], P. Sherwood[15], G.P. Siroli[2], A. Skillman[16], A. Skuja[17], A.M. Smith[8], T.J. Smith[28], G.A. Snow[17], R. Sobie[28], R.W. Springer[17], M. Sproston[20], A. Stahl[3], C. Stegmann[10], K. Stephens[16], J. Steuerer[28], R. Ströhmer[11], D. Strom[19], H. Takeda[24], S. Tarem[8], M. Tecchio[9], P. Teixeira-Dias[11], N. Tesch[3], M.A. Thomson[15], E. Torrente-Lujan[22], S. Towers[6], N.J. Tresilian[16], T. Tsukamoto[24],

M.F. Turner[8], D. Van den plas[18], R. Van Kooten[12], G.J. VanDalen[4], G. Vasseur[21], M. Vincter[28], A. Wagner[27], D.L. Wagner[9], C. Wahl[10], C.P. Ward[5], D.R. Ward[5], J.J. Ward[15], P.M. Watkins[1], A.T. Watson[1], N.K. Watson[7], P. Weber[6], P.S. Wells[8], N. Wermes[3], B. Wilkens[10], G.W. Wilson[4], J.A. Wilson[1], V-H. Winterer[10], T. Wlodek[26], G. Wolf[26], S. Wotton[11], T.R. Wyatt[16], R. Yaari[26], A. Yeaman[13], G. Yekutieli[26], M. Yurko[18], W. Zeuner[8], G.T. Zorn[17].

[1]School of Physics and Space Research, University of Birmingham, Birmingham B15 2TT, UK
[2]Dipartimento di Fisica dell' Università di Bologna and INFN, I-40126 Bologna, Italy
[3]Physikalisches Institut, Universität Bonn, D-53115 Bonn, Germany
[4]Department of Physics, University of California, Riverside CA 92521, USA
[5]Cavendish Laboratory, Cambridge CB3 0HE, UK
[6]Carleton University, Department of Physics, Colonel By Drive, Ottawa, Ontario K1S 5B6, Canada
[7]Centre for Research in Particle Physics, Carleton University, Ottawa, Ontario K1S 5B6, Canada
[8]CERN, European Organisation for Particle Physics, CH-1211 Geneva 23, Switzerland
[9]Enrico Fermi Institute and Department of Physics, University of Chicago, Chicago IL 60637, USA
[10]Fakultät für Physik, Albert Ludwigs Universität, D-79104 Freiburg, Germany
[11]Physikalisches Institut, Universität Heidelberg, D-69120 Heidelberg, Germany
[12]Indiana University, Department of Physics, Swain Hall West 117, Bloomington IN 47405, USA
[13]Queen Mary and Westfield College, University of London, London E1 4NS, UK
[14]Birkbeck College, London WC1E 7HV, UK
[15]University College London, London WC1E 6BT, UK
[16]Department of Physics, Schuster Laboratory, The University, Manchester M13 9PL, UK
[17]Department of Physics, University of Maryland, College Park, MD 20742, USA
[18]Laboratoire de Physique Nucléaire, Université de Montréal, Montréal, Quebec H3C 3J7, Canada
[19]University of Oregon, Department of Physics, Eugene OR 97403, USA
[20]Rutherford Appleton Laboratory, Chilton, Didcot, Oxfordshire OX11 0QX, UK
[21]DAPNIA/SPP, Saclay, F-91191 Gif-sur-Yvette, France
[22]Department of Physics, Technion-Israel Institute of Technology, Haifa 32000, Israel
[23]Department of Physics and Astronomy, Tel Aviv University, Tel Aviv 69978, Israel
[24]International Centre for Elementary Particle Physics and Department of Physics, University of Tokyo, Tokyo 113, and Kobe University, Kobe 657, Japan
[25]Brunel University, Uxbridge, Middlesex UB8 3PH, UK
[26]Particle Physics Department, Weizmann Institute of Science, Rehovot 76100, Israel
[27]Universität Hamburg/DESY, II Institut für Experimental Physik, Notkestrasse 85, D-22607 Hamburg, Germany
[28]University of Victoria, Department of Physics, P O Box 3055, Victoria BC V8W 3P6, Canada
[29]University of British Columbia, Department of Physics, Vancouver BC V6T 1Z1, Canada
[30]University of Alberta, Department of Physics, Edmonton AB T6G 2J1, Canada
[31]Duke University, Dept of Physics, Durham, NC 27708-0305, USA
[32]Universität Aachen, III Physikalisches Institut, Sommerfeldstrasse 26-28, D-52056 Aachen, Germany

[a]Also at TRIUMF, Vancouver, Canada V6T 2A3

1 Introduction

The knowledge of the hadronic particle composition of the $q\bar{q}$ final state in e^+e^- annihilation is important for understanding the fragmentation of quarks and gluons into hadrons. No exact theoretical prescription exists for this process yet. Instead, a variety of phenomenological models have been developed. At present, those used most commonly are the string fragmentation model [1] and the cluster fragmentation model [2]. Another approach to describing the hadron momentum spectra combines the modified leading log approximation (MLLA) [3] of QCD with the concepts of local parton hadron duality (LPHD) [4].

In this paper measurements of the momentum spectra of the charged hadrons $\pi^{\pm}$, $K^{\pm}$ and $p\bar{p}$ resulting from Z^0 decays into multihadronic final states at centre of mass energies E_{CM} of 91.2 GeV are presented. The data obtained are then compared with predictions from the JETSET [5] and the HERWIG [6] Monte Carlo generators with optimized parameters[1] [7], representing the string and the cluster fragmentation models, respectively. Similar measurements in e^+e^- annihilations at $\sqrt{s} = 10$ GeV [8, 9] and around $\sqrt{s} = 29$ GeV [10, 11, 12, 13] have been previously reported.

Production rates of neutral pions and η at LEP have been published by the L3 collaboration [14, 15]. Neutral kaon and lambda production rates have been published by the OPAL [16, 17] and the DELPHI collaborations [18]. Production rates for $K^*(892)^{\pm}$ and Ξ^- have been published by the OPAL collaboration [19, 17]. These data are used later for comparison with the MLLA predictions and the predictions of the JETSET and HERWIG Monte Carlo generators.

2 The OPAL Detector

The OPAL detector has been described in detail elsewhere [20]. It is a multipurpose detector covering almost the entire solid angle around the interaction region at LEP. Its main parts are a system of central tracking chambers inside a magnetic field of 0.435 T, an electromagnetic calorimeter, a hadron calorimeter and an outer shell of muon chambers.

In the present analysis, only information from the tracking chambers is used. Three sets of drift chambers allow an accurate determination of the vertex of the interaction and of charged particle momenta. The chamber closest to the beam is the vertex chamber, which measures the coordinates with resolutions of $\sigma_{r\phi} \approx 50$ μm and $\sigma_z \approx 700$ μm.[2] The main part of the tracking system is a jet chamber of about 2 m in radius and 4 m in length. It is divided into 24 sectors in ϕ, each equipped with 159 sense wires. Up to 159 measurements per track per sector are possible with a precision of $\sigma_{r\phi} \approx 135$ μm from timing information and $\sigma_z \approx 6$ cm from charge division. A precise measurement of the z-coordinate is provided by a set of drift chambers (Z-chambers)

[1] "JETSET" and "HERWIG" throughout this paper stand for "JETSET 7.3 and HERWIG 5.5 with optimized parameters tuned by OPAL in order to decribe the measured global event shape distributions" unless otherwise indicated.

[2] A right-handed coordinate system is adopted by OPAL, where the x axis points to the centre of the LEP ring, and positive z is along the electron beam direction. The angles θ and ϕ are the polar and azimuthal angles, respectively.

located at a radius of 192 cm from the interaction point, yielding up to six measurements with a single hit resolution of $\sigma_z \approx 300$ μm. The combination of these chambers leads to a momentum resolution of $\sigma_{p_t}/p_t \approx \sqrt{0.02^2 + (0.0015 \cdot p_t)^2}$ (p_t is the transverse momentum in GeV/c), where the first term represents the contribution from multiple scattering.

Particles are identified by the simultaneous measurement of momentum p and energy loss $\mathrm{d}E/\mathrm{d}x$ in the jet chamber (fig. 1). A detailed description of the energy loss measurement can be found in [21]. The resolution achieved in multihadronic events is $\sigma(\mathrm{d}E/\mathrm{d}x)/(\mathrm{d}E/\mathrm{d}x) = 3.5\%$ for 159 charge samples on a track. This allows a separation with two standard deviations significance of pions and kaons up to 24 GeV/c for tracks with at least 100 measured samples (fig. 2).

3 Event and Track Selection

The data used in this analysis correspond to an integrated luminosity of 24.9 pb^{-1} collected in 1992. After the selection of multihadronic events, 766 016 events remain. This selection accepts $(98.37 \pm 0.21)\%$ of multihadronic events and is described in detail in [22]. Remaining background processes, such as $\mathrm{e^+e^-} \to \tau^+\tau^-$, are estimated to be at a level of less than 0.1%.

Tracks are required to have a minimum transverse momentum with respect to the beam direction of 0.15 GeV/c. They are accepted if their distance of closest approach to the event vertex in the plane transverse to the beam direction is less than 5 cm ($|d_0| < 5$ cm) and if their distance from the event vertex along the beam direction at the distance of closest approach is less than 40 cm ($|z_0| < 40$ cm). This reduces the number of tracks from nuclear interactions and keeps most of the tracks from decays of short lived particles ($\tau < 3 \cdot 10^{-10}$ s); therefore, corrections in the subsequent analysis are kept small.

Each track is required to have a minimum of 100 hits in the jet chamber used for determination of the energy loss $\mathrm{d}E/\mathrm{d}x$ and a match of the track to the Z-chambers. The first condition ensures a $\mathrm{d}E/\mathrm{d}x$ resolution of better than 4.0% for tracks in multihadronic events. The second condition is required to obtain a good resolution of the polar angle θ, but restricts the clean acceptance region to $|\cos\theta| < 0.7$ due to the limited coverage of the Z-chambers. To improve the resolution in θ further, all tracks with $|d_0| \leq 5$ mm are constrained to the event vertex in z. The radial position of the first measured point of a track in the jet chamber is required to be less than 60 cm. With these conditions 22.1% of all tracks are retained.

4 Measurement of Particle Fractions

4.1 $\mathrm{d}E/\mathrm{d}x$ Measurement

For the determination of the charged hadron fractions the simultaneous measurement of momentum p and specific energy loss $\mathrm{d}E/\mathrm{d}x$ in the jet chamber is used (fig. 1). The energy loss of particles in matter is described by the Bethe-Bloch equation [23] and is a universal function of $\beta\gamma = p/m$ for all particle masses. The energy loss as a function of momentum shows

a characteristic decrease as $1/\beta^2$, reaches a minimum around $\beta\gamma \approx 4$, and continues with a logarithmic rise ("relativistic rise region") until it saturates ("Fermi plateau"). Typically the $\mathrm{d}E/\mathrm{d}x$ increase from the minimum up to the plateau is of the order of 40–70% for commonly used drift chamber gases (47% for the OPAL jet chamber). The energy loss distribution of a charged particle traversing matter has a large inherent width of 60–70% (FWHM) for a path length of 1 cm in gas at atmospheric pressure. Sufficient accuracy can be achieved by measuring many samples along a track.

The jet chamber is operated at a pressure of 4 bar with a nominal sampling length of 1 cm. It provides a maximum of 159 three-dimensional points (r, ϕ, z) per track, together with charge deposition measurements. The measured raw charges are subject to quality cuts and corrections. Hits from two very close-by tracks (< 1 cm distance) and hits close to chamber boundaries are rejected. The charge of all remaining hits is corrected for individual wire and electronic gains, crosstalk effects, gas gain saturation, geometric path length and long term gas gain variations. The corrections are discussed in detail in [21].

After application of all corrections, the specific energy loss $\mathrm{d}E/\mathrm{d}x$ is calculated by the method of truncated mean [24] where the highest 30% of the energy loss measurements of a track are discarded, while the mean value of the lower 70% is taken to be the specific energy loss of the track. The $\mathrm{d}E/\mathrm{d}x$ resolution obtained for the maximum number of 159 possible hits was found to be 3.0% for isolated tracks from muon pairs and 3.5% for tracks from minimum ionizing pions within multihadronic events.

4.2 Particle Identification

In order to determine the differential cross sections for the different particle species, the track sample was divided into 68 momentum intervals ranging from 0.22 to 45.6 GeV/c. The widths of the intervals were chosen such that the number of tracks in each bin was similar.

As seen in figs. 1 and 3a the particle species are well separated in $\mathrm{d}E/\mathrm{d}x$ for low momenta. The tracks are identified individually and their relative rates are obtained by counting. The minimum in the $\mathrm{d}E/\mathrm{d}x$ distribution between two particle species is used as a cut to distinguish between the two corresponding particle species. Corrections due to overlaps are negligible.

Particle identification between 1.4 and 2.0 GeV/c is difficult because the mean energy loss functions for pions, kaons and protons cross one another as seen in fig. 1. Above 2.0 GeV/c pions are separated from kaons/protons and above 4.0 GeV/c pions, kaons and protons are again separated sufficiently up to the maximum momentum of 45.6 GeV/c. However, the separation for high momenta (the relativistic rise) is of the order of about two to three standard deviations for pions and kaons and less than two standard deviations for kaons and protons (fig. 2). Therefore, an unambiguous individual identification is not possible and a statistical method has to be applied.

In each of these momentum intervals, the number of particles N_i of each species ($i = \mathrm{e}^{\pm}$, $\pi^{\pm}$, $\mathrm{K}^{\pm}$, $\mathrm{p\bar{p}}$) is obtained by a simultaneous χ^2 fit of four overlapping functions representing the $\mathrm{d}E/\mathrm{d}x$ distributions of the four individual particle species (fig. 3b). The individual particle rate is then calculated from the area of the corresponding $\mathrm{d}E/\mathrm{d}x$ distribution. The small energy loss difference between pions and muons does not allow a separation of these two particle species.

Pions are therefore contaminated by muons, but corrections are made for this contamination later. Particles and antiparticles are not distinguished in the quoted rates.

The simultaneous fit of four functions requires a precise knowledge of the functional form of the individual $\mathrm{d}E/\mathrm{d}x$ distribution of a single particle type. Even in the simplest case where each of the individual $\mathrm{d}E/\mathrm{d}x$ distributions is assumed to be a Gaussian function, this would lead to 4×3 free parameters. Since the number of pions expected is much larger than the number of kaons and protons, a completely unconstrained fit is unstable, so that some parameters have to be fixed. Furthermore, the individual $\mathrm{d}E/\mathrm{d}x$ distribution for a single particle species in a certain momentum interval is not well modelled by a single Gaussian function, but requires a more precise description, as discussed in the next section.

4.3 Individual $\mathrm{d}E/\mathrm{d}x$ Distribution

The $\mathrm{d}E/\mathrm{d}x$ resolution of tracks varies with the number of usable $\mathrm{d}E/\mathrm{d}x$ hits ($N_{\mathrm{d}E/\mathrm{d}x}$) and with the path length l of an individual charge sample, which leads to a significant improvement at large $\cos\theta$. For isolated tracks, about 7.5% of the hits are rejected by cuts on the quality of the raw charge measurement as described in [21], whereas for tracks within multihadronic events about 31.5% are not usable for the calculation of the energy loss, resulting in a better resolution for isolated tracks. The relative $\mathrm{d}E/\mathrm{d}x$ resolution for isolated tracks was measured to be

$$\left(\frac{\sigma_{\mathrm{d}E/\mathrm{d}x}}{\mathrm{d}E/\mathrm{d}x}\right)_{\mathrm{isolated}} = 0.030 \cdot \left(\frac{N_{\mathrm{d}E/\mathrm{d}x}}{159}\right)^{-0.45} \cdot l^{-0.32} \qquad l \text{ in cm.} \tag{1}$$

In addition to the number of hits and the path length, the resolution also depends on the track environment. The charge measurement of a single hit in a dense track environment is less precise than that of a hit of an isolated track because of crosstalk from other hits. The amount of crosstalk depends on the density of tracks within a jet chamber sector and a variable giving a good measure of this effect is found to be the total sum of deposited charge, Q_{dep}, of all other hits in that specific sector. The deposited charge of tracks passing two or more jet chamber sectors is weighted according to the number of track hits in each sector. Q_{dep} and the number of usable $\mathrm{d}E/\mathrm{d}x$ hits per track are strongly correlated and the overall $\mathrm{d}E/\mathrm{d}x$ resolution in a dense track environment was found to vary linearly with the deposited charge Q_{dep}:

$$\left(\frac{\sigma_{\mathrm{d}E/\mathrm{d}x}}{\mathrm{d}E/\mathrm{d}x}\right)_{\mathrm{dense}} = (1 + 0.046 \cdot Q_{\mathrm{dep}}) \cdot \left(\frac{\sigma_{\mathrm{d}E/\mathrm{d}x}}{\mathrm{d}E/\mathrm{d}x}\right)_{\mathrm{isolated}} \qquad Q_{\mathrm{dep}} \text{ in MeV.} \tag{2}$$

Typical average values of Q_{dep} for multihadronic events are equivalent to 4–7 MeV and correspond to $\sigma(\mathrm{d}E/\mathrm{d}x)/(\mathrm{d}E/\mathrm{d}x) = 3.6$–$4.0\%$ or about 0.15% loss in resolution per 1 MeV of Q_{dep}.

The individual $\mathrm{d}E/\mathrm{d}x$ distribution for a single particle species in a given momentum interval is comprised of an overlay of a number of Gaussians, each with the same central value but with different widths depending on the $N_{\mathrm{d}E/\mathrm{d}x}$ and Q_{dep} distributions. The shape of the resulting $\mathrm{d}E/\mathrm{d}x$ distribution varies with momentum. Low momentum tracks have a small $\langle Q_{\mathrm{dep}} \rangle$ compared to high momentum tracks. These low momentum tracks have a smaller radius of curvature and leave the particle jet cone after a short flight distance and are therefore more

isolated. Q_{dep} distributions for two momentum intervals are shown in figs. 4a and 4b. For each momentum interval where a combined fit for four particle species has to be performed, the shape of the individual $\mathrm{d}E/\mathrm{d}x$ distribution has to be known.

In order to obtain accurate individual $\mathrm{d}E/\mathrm{d}x$ distributions, only minimum ionizing pions (0.45 to 0.65 GeV/c) can be used as they are well separated from all other particle species. The shape of the $\mathrm{d}E/\mathrm{d}x$ distribution was studied as a function of Q_{dep}. The entire Q_{dep} spectrum was subdivided into 50 intervals each 0.5 MeV wide. Within each interval the shape of the single $\mathrm{d}E/\mathrm{d}x$ distribution is well described by a single Gaussian function with approximately the same central value for all intervals.

However, the widths of the single distributions increase with larger track density Q_{dep} as expected from the discussion above. The resulting total $\mathrm{d}E/\mathrm{d}x$ distribution is obtained from the sum of all single distributions weighted according to the Q_{dep} distribution. The $\mathrm{d}E/\mathrm{d}x$ distributions for all other momentum intervals are also obtained from the sum of all single distributions derived from minimum ionizing pions. However, these are weighted according to the Q_{dep} distribution for the momentum interval in question.

This sum of single distributions can be parameterized for each momentum interval adequately by a double Gaussian function as indicated in figs. 4c and 4d. In order to allow a possible asymmetry due to calibration imperfections the central values of both Gaussians are allowed to differ slightly. This parameterization by a double Gaussian was checked with data and with the detector simulation program GOPAL [25] using the JETSET generator. The integral of the double Gaussians agrees to within 0.06% with the sum over all single distributions.

The expected mean $\langle \mathrm{d}E/\mathrm{d}x \rangle$ for electrons, pions, kaons and protons in each momentum interval was obtained from data by a fit based on a parametrisation derived by Sternheimer and Peierls [26] with additional corrections [21]. For momenta below 1.4 GeV/c data from all particle species are used, whereas in the relativistic rise region above 2.0 GeV/c only pions are taken due to the limited particle separation power. The widths of the residual distributions $(\mathrm{d}E/\mathrm{d}x)_{\mathrm{measured}} - (\mathrm{d}E/\mathrm{d}x)_{\mathrm{fitted}}$ at low momenta are less than 0.2% for pions and 0.5% for kaons and protons.

Each double Gaussian G_i characterizing the individual $\mathrm{d}E/\mathrm{d}x$ distribution of a single particle species in a certain momentum interval is defined as:

$$
\begin{aligned}
G_i(s,\sigma;\mathrm{d}E/\mathrm{d}x) \;=\; & \exp\left[-\frac{1}{2}\left(\frac{\mathrm{d}E/\mathrm{d}x - s\cdot\langle \mathrm{d}E/\mathrm{d}x\rangle_i}{s\cdot\langle \mathrm{d}E/\mathrm{d}x\rangle_i\cdot\sigma}\right)^2\right] \;+ \\
& g_c\cdot\exp\left[-\frac{1}{2}\left(\frac{\mathrm{d}E/\mathrm{d}x - s\cdot\langle \mathrm{d}E/\mathrm{d}x\rangle_i - g_m\cdot s\cdot\langle \mathrm{d}E/\mathrm{d}x\rangle_i\cdot\sigma}{g_\sigma\cdot s\cdot\langle \mathrm{d}E/\mathrm{d}x\rangle_i\cdot\sigma}\right)^2\right] \quad . \quad (3)
\end{aligned}
$$

where $\langle \mathrm{d}E/\mathrm{d}x\rangle_i$ is the expected mean $\mathrm{d}E/\mathrm{d}x$ for particle species i in the momentum interval, σ is the relative $\mathrm{d}E/\mathrm{d}x$ resolution, s is a scaling factor allowing a variation of the expected mean $\mathrm{d}E/\mathrm{d}x$, g_c is the ratio of the heights, g_m is the shift of the second Gaussian in terms of σ, and g_σ is the ratio of the widths. In table 1 the relations between the first Gaussian and the second Gaussian for some momentum intervals are shown.

Pions from $\mathrm{K}^0_{\mathrm{S}} \to \pi^+\pi^-$ decays were used to verify the correct description of the shape of the $\mathrm{d}E/\mathrm{d}x$ distribution in the relativistic rise region. Fig. 5 shows the normalised $\mathrm{d}E/\mathrm{d}x$ distribu-

tion $(\mathrm{d}E/\mathrm{d}x_{\mathrm{measured}} - \mathrm{d}E/\mathrm{d}x_{\mathrm{expected}})/\sigma(\mathrm{d}E/\mathrm{d}x)$ of these pions above 2.0 GeV/c together with the result of a single Gaussian fit. The figure indicates that the $\mathrm{d}E/\mathrm{d}x$ error function is well represented by a unit Gaussian over three orders of magnitude. Using Monte Carlo events it was checked that the number of usable $\mathrm{d}E/\mathrm{d}x$ hits and the deposited charge Q_{dep} representing the track density do not depend on the particle species. Thus, pions, kaons and protons do not differ in the shape of their $\mathrm{d}E/\mathrm{d}x$ distributions.

4.4 Fitting Procedure

In each momentum interval above 2.0 GeV/c, a χ^2 fit was performed to the measured $\mathrm{d}E/\mathrm{d}x$ distribution representing the superposition of the four individual $\mathrm{d}E/\mathrm{d}x$ distributions from the 4 particle species and parametrised as double Gaussians (fig. 3b).

In total, 8 parameters were fitted for each momentum bin:

$$N(\mathrm{d}E/\mathrm{d}x) = c_{\mathrm{e}} \cdot G_{\mathrm{e}}(s,\sigma) + c_{\pi} \cdot G_{\pi}(s,\sigma) + c_{\mathrm{K}} \cdot G_{\mathrm{K}}(s \cdot s_{\mathrm{K}},\sigma) + c_{\mathrm{p}} \cdot G_{\mathrm{p}}(s \cdot s_{\mathrm{p}},\sigma) \quad , \qquad (4)$$

where

- c_{e},c_{π},c_{K},c_{p} are the heights of the four double Gaussians G_i;
- σ is the relative $\mathrm{d}E/\mathrm{d}x$ resolution which is taken to be the same for the four double Gaussians;
- s is a scale factor allowing a single common variation for the mean $\mathrm{d}E/\mathrm{d}x$ for all four particle species; and
- s_{K} and s_{p} are scale factors allowing separate variations for the mean $\mathrm{d}E/\mathrm{d}x$ for kaons and for protons relative to the mean $\mathrm{d}E/\mathrm{d}x$ of pions in the unresolved region above 2 GeV/c.

Only one relative $\mathrm{d}E/\mathrm{d}x$ resolution is used for the four double Gaussians since the variation of the mean $\mathrm{d}E/\mathrm{d}x$ within one momentum interval shows nearly the same slope for all particle species above 4 GeV/c and therefore has the same influence on the width of the $\mathrm{d}E/\mathrm{d}x$ distribution. The values of the fitted scale factors s, s_{K} and s_{p} are compatible with the size of the residuals of the $\mathrm{d}E/\mathrm{d}x$ parametrisation described above.

The rates for the four particle species are determined by the integrals of their individual $\mathrm{d}E/\mathrm{d}x$ distributions with the parameters resulting from the combined fit. Further corrections are then applied. Although four double Gaussians including the electrons are fitted, rates will be given only for the three hadron species. A large number of low-momentum electrons originate from photon conversions and would need to be subtracted. This correction would increase the size of the systematic error of the electron rates to an unacceptably high level.

4.5 Efficiency and Corrections

Momentum dependent efficiency corrections are made that take into account the effects of geometrical and kinematic acceptance, nuclear interactions and decays in flight. All these

corrections have been determined using Monte Carlo events. The efficiency typically varies between 20 and 30% for the cuts described above. All cut distributions in data and Monte Carlo have been compared and no significant differences have been seen, except for the match of the tracks to the Z-chambers. The Z-chamber matching efficiency is slightly lower in data than in Monte Carlo and this difference has been corrected as a function of momentum.

The measured particle rates obtained by counting below 1.4 GeV/c and by the combined fit above 2.0 GeV/c are corrected for the momentum dependent track selection and reconstruction efficiency. Low momentum negatively charged tracks are well described by the detector simulation program, whereas there are discrepancies for low momentum positively charged tracks. This is partly due to the inaccurate modelling of tracks from nuclear interactions. Therefore, only negatively charged particles are considered for momenta below 1.4 GeV/c, and these rates are doubled to obtain the total rates.

As seen in fig. 1 the $\mathrm{d}E/\mathrm{d}x$ of kaons in the momentum range of 0.5 to 0.8 GeV/c and the $\mathrm{d}E/\mathrm{d}x$ of protons in the momentum range of 0.9 to 1.4 GeV/c cross over the $\mathrm{d}E/\mathrm{d}x$ of electrons. This electron contamination has been corrected as follows. The electron rates for momenta above, below and between the kaon/proton crossings have been determined. In these momentum ranges the electrons are well separated from the kaons and protons. To estimate the electron contamination for the kaon and proton momentum bins in question, the electron rates have been interpolated and subtracted. The errors due to the interpolation have been included in the systematic errors.

As mentioned above, pions cannot be separated from muons; instead the muon rate is subtracted from the pion rate according to the predictions of JETSET. The muon rate is typically between 2 and 5% of the pion rate and depends slightly on momentum. It has been verified by Monte Carlo that the change in the shape of the pion $\mathrm{d}E/\mathrm{d}x$ distribution due to the muon contamination is negligible.

To allow comparisons with lower energy data, decays of particles with mean lifetimes greater than $3 \cdot 10^{-10}$ s are not counted when determining the Monte Carlo efficiency. In consequence, the pion fractions include contributions from K^0_S decays, but not from K^0_L and $\mathrm{K}^\pm$ decays, and the proton fractions include contributions from Λ decays.

Systematic shifts in the momentum measurement have been investigated with Monte Carlo events. The difference between real and reconstructed momenta due to energy loss depends on momentum and particle type. For $p > 2.0$ GeV/c the energy loss is always less than 10 keV/cm. Therefore, corrections for these momentum bins are small and nearly the same for each particle species. For $p < 1.4$ GeV/c the energy loss becomes larger and the correction is a function of momentum and particle type (fig. 1). These correction factors are taken from Monte Carlo for each particle species.

5 Systematic Errors and Checks

A summary of the systematic errors is given in table 2. Most of them vary with momentum. To indicate their typical size, only their mean values are given in table 2.

The following systematic errors are applied to each momentum bin in the entire momentum range investigated:

- **Track selection cuts**
  The entire analysis has been repeated for several combinations of track selection cuts:

  The $\mathrm{d}E/\mathrm{d}x$ hit cuts used were $N_{\mathrm{d}E/\mathrm{d}x} \geq 80$, ≥ 100, ≥ 120 and two uncorrelated data sets with $80 \leq N_{\mathrm{d}E/\mathrm{d}x} \leq 110$ and $N_{\mathrm{d}E/\mathrm{d}x} > 110$. The d_0 cuts used were $|d_0| < 0.5$ and 5 cm. The R.M.S. of the difference between the rates obtained for these variations and the rates for the nominal cuts ($N_{\mathrm{d}E/\mathrm{d}x} \geq 100$ and $|d_0| < 5$ cm) are 0.2% (0.6%) for pions, 2.2% (1.0%) for kaons and 3.4% (5.4%) for protons where the first error is for $p < 1.4$ GeV/c and the error in brackets is for $p > 2.0$ GeV/c. All other variations of track selection cuts result in negligible influence ($< 0.5\%$).

- **Muon subtraction**
  Under the assumption that the muon rates are described to better than $\pm 10\%$ in the JETSET Monte Carlo [27], the error on the pion rates caused by the muon subtraction is of the order of $\pm 0.5\%$. No effort to identify muons using the muon chambers is made because the systematic error due to misidentification and track matching to the muon chamber hits is larger than the error from the muon subtraction.

- **Momentum correction for energy loss in detector material**
  The systematic error due to the momentum correction has been studied using pions from K^0_S decays. Due to the energy loss in material between the decay point and the jet chamber, the reconstructed $\pi^+\pi^-$ invariant mass is systematically too small for low momentum K^0_S. Applying the energy loss correction to the momenta removes the discrepancy. The losses in the material are thus well modelled by the Monte Carlo.

For momentum bins below 1.4 GeV/c :

- **Counting method**
  The fitting procedure was extended to the low-momentum intervals and no significant differences in the measured rates was observed.

- **Nuclear interactions**
  The fraction of tracks due to nuclear interactions is estimated with the Monte Carlo and removed from the measured rates. This fraction was about 10%. Studies of the distributions of track parameters, such as the d_0, suggest that the number of tracks originating from nuclear interactions could be over– or under–estimated by at most 20%, resulting in errors on the pion, kaon and proton rates of 2.8%, 0.6% and 1.0%, respectively.

- **Decays in flight**
  The corrections for decays in flight are of the order of 3% for pions and of 8% for kaons. The systematic errors due to these corrections are 0.2% for the pion rates and 0.2% for the kaon rates.

- **Electron subtraction**
  The systematic error due to electron subtraction in the cross-over regions of kaons and protons has been studied using Monte Carlo events. The maximum error in the momentum bins with largest electron contamination results in 5% for kaons and 10% for protons. The systematic error in other momentum bins is scaled down proportional to the contamination.

For momentum bins above 2.0 GeV/c :

- **Fit method**
  The described fit method has been varied in several ways.

  First the method has been applied to Monte Carlo events and the reproduction of the rates has been tested. This results in a systematic error due to the fit method of 0.2% for pions, 0.5% for kaons and 0.4% for protons.

  As a further test, the measured pion distribution has been subtracted from the data and the fit procedure repeated for kaons and protons only. Also the number of fit parameters has been altered. Instead of one common relative resolution for $\pi^{\pm}$, $\mathrm{K}^{\pm}$ and $\mathrm{p\bar{p}}$, fits with two and three relative resolutions have been performed. These variations of the fit method result in systematic errors of 1.1% for pions, 2.7% for kaons and 7.3% for protons.

  Finally, using an unbinned maximum likelihood method instead of a χ^2 fit results in variations of 0.8% for pions, 0.9% for kaons and 6.2% for protons.

  Adding all these results in quadrature for each particle species, total systematic errors for the fit method are on average 1.4% for pions, 2.9% for kaons and 9.6% for protons. However, the systematic errors are larger close to a cross-over region in $\mathrm{d}E/\mathrm{d}x$.

- **Scale factors and relative resolutions**
  The scale factors fitted to the mean $\mathrm{d}E/\mathrm{d}x$ of each particle species are of the order of 1.00 ± 0.01. These values have been checked with pions from $\mathrm{K}^0_{\mathrm{S}} \to \pi^+\pi^-$ decays and with protons from $\Lambda^0 \to \mathrm{p}\pi$ decays. The mean $\mathrm{d}E/\mathrm{d}x$ of the tagged pion and proton samples agree well with the scale values of the fit.

  An additional test was performed using Monte Carlo events. The $\mathrm{d}E/\mathrm{d}x$ of kaons and protons was shifted artificially with respect to the $\mathrm{d}E/\mathrm{d}x$ of pions and the fit repeated. The resulting scaling factors, s_{K} and s_{p}, followed the artificial shift and the rates were reproduced up to a shift of 1%.

  In the momentum bins with sufficient $\mathrm{d}E/\mathrm{d}x$ separation it has been verified with Monte Carlo events and data that the relative resolution is independent of the particle type to the level of 5%. Since the relative resolution in the fits is mainly fixed by the pion distribution, this results in a systematic error of 5% for the kaon and proton rates. An error of 1% is taken for the pion rates because of feedback to the fitted pion resolution from kaon and proton resolutions.

- **Double Gaussian representation**
  To check the dependence of the rates on the description of the energy loss distribution by the double Gaussian, all parameters of the second Gaussian have been varied individually and in combination up to 20%. These variations are much larger than the observed

differences between the double Gaussian functions and the sum of the individual Gaussians in the description of the $\mathrm{d}E/\mathrm{d}x$ distribution (0.06%, see section 4.3). They take into account possible momentum dependent shape changes. The resulting rate changes are 0.7% for pions, 1.6% for kaons and 9.9% for protons.

For the parametrisation of the double Gaussians as well as for the determination of the particle rates, tracks in multihadronic events are used with identical cuts and therefore, are selected within the same track environment. The mean number of hits $N_{\mathrm{d}E/\mathrm{d}x}$ in a given momentum interval turns out to be the same within one hit for pion, kaon and proton candidates as checked using Monte Carlo events. This indicates that there should be negligible systematic errors resulting from possibly different track environments for different particle types.

- **Starting values**
  The starting values used as input to the fitting algorithm for the mean energy loss are derived from the parametrisation of the energy loss function; for the relative resolution and the scale factors, starting values of 4.0% and 1.0 respectively are taken. The initial values of the heights of the Gaussians are obtained from the scaled Monte Carlo prediction. All starting values have been varied individually and in combination (up to $\pm 20\%$) and rate changes for pions of 2.1%, for kaons of 0.4% and for protons of 1.8% have been measured.

Adding all systematic errors in quadrature for each particle species results in average total errors of 2.9/2.5/4.1% for $p < 1.4$ GeV/c and 3.0/6.1/15.7% for $p > 2.0$ GeV/c for pions/kaons/protons (see table 2). Due to the nature of the fitting method, systematic errors above $p > 2.0$ GeV/c are highly correlated between the three particle species. A systematic shift e.g. in the mean $\mathrm{d}E/\mathrm{d}x$ of kaons results in a change of the measured kaon rate and a corresponding correlated change of the proton and pion rates.

6 Results and Discussion

The normalized rates of pions ($\pi^{\pm}$), kaons ($\mathrm{K}^{\pm}$) and protons ($\mathrm{p\bar{p}}$) obtained in each momentum interval are listed in tables 3, 4 and 5 together with their statistical and systematic errors. The momentum distributions are shown in fig. 6 together with the predictions of the JETSET and the HERWIG generators and the ratios between data and predictions.[3] The differential cross sections $1/(\sigma_{\mathrm{had}}\beta)(\mathrm{d}\sigma/\mathrm{d}x_E)$ are shown in fig. 7 as a function of x_E ($x_E = 2 \cdot E/\sqrt{s}$). The predictions of the JETSET and the HERWIG generators are also shown.

The generators are tuned in such a way that the global event shape distributions agree with the data [7]. The total charged track multiplicities for the tuned generators are approximately equal to the data. Therefore, a difference in the production rate of one particle species implies a corresponding difference in the production rates of other species. This is most obvious when one compares the measured data with the prediction of the HERWIG generator for momenta below 2.0 GeV/c. The HERWIG prediction for the kaon cross section is significantly larger

[3]The Monte Carlo predictions are obtained in the same way as the data. The momentum spectra are subdivided into 68 momentum intervals. Then, the cross sections as function of the weighted mean momentum in each momentum interval are fitted by a polynomial.

than the measurement, as seen in fig. 6b. Given that the predicted cross section of charged particles [28] and charged pions are in good agreement with the data (fig. 6a), the excess in the charged kaon cross section is compensated by a reduced proton cross section, as seen in fig. 6c.

For data above 2.0 GeV/c, similar correlations between the particle rates within a particular momentum interval are due to the fitting method. As described in section 5 these correlations are covered by the quoted systematic errors and therefore cannot account for the discrepancy between data and the generators.

The cross sections as a function of momentum and of x_E as predicted by JETSET are in good agreement with the data for pions ($\pi^{\pm}$) in the observed regions. Deviations are observed both for JETSET and HERWIG for kaons ($\mathrm{K}^{\pm}$), where at high momenta the measured cross sections are larger than the predicted ones. For protons ($\mathrm{p\bar{p}}$) the measured cross sections are smaller than the predicted ones. The same behaviour has been observed for Λ production [17].

In order to determine the total rates of the different hadron species, the cross sections $1/(\sigma_{\mathrm{had}}\beta)(\mathrm{d}\sigma/\mathrm{d}x_E)$ are integrated, using a smooth function to interpolate in the cross-over region and using the Monte Carlo to extrapolate into the unobserved low momentum regions. The extrapolation yields 1.166 ± 0.023 $\pi^{\pm}$, 0.034 ± 0.002 $\mathrm{K}^{\pm}$ and 0.024 ± 0.005 $\mathrm{p\bar{p}}$ per multihadronic event where the errors include both statistical and systematic contributions. For interpolation of the cross-over regions an exponential of a polynomial in x_E describing the JETSET Monte Carlo shape was fitted to the data (fig. 7) and the total rates calculated by integrating the fitted function over the unobserved region.

To estimate the systematic error of the interpolation, this function has also been fitted to the same Monte Carlo momentum intervals as for the data and the obtained rates have been compared to the generated rates. The interpolation procedure for the data has been repeated with one standard deviation systematic error added or subtracted under the conservative assumption of full correlation between all points. In addition, the Monte Carlo function has been fitted to the data with only one scale factor as a free parameter. The total systematic error due to interpolation is derived by adding these three deviations in quadrature.

All rates, including the ones from the measured momentum regions, are summarized in table 6. Again assuming fully correlated systematic errors between different momentum intervals, the systematic errors are added linearly.

The total rates per multihadronic event are: 17.05 ± 0.43 pions ($\pi^{\pm}$), 2.42 ± 0.13 kaons ($\mathrm{K}^{\pm}$) and 0.92 ± 0.11 protons ($\mathrm{p\bar{p}}$). This can be compared with the JETSET predictions of 16.992 ± 0.005 ($\pi^{\pm}$), 2.258 ± 0.002 ($\mathrm{K}^{\pm}$) and 1.145 ± 0.001 ($\mathrm{p\bar{p}}$) and the HERWIG predictions of 17.754 ± 0.008 ($\pi^{\pm}$), 2.471 ± 0.003 ($\mathrm{K}^{\pm}$) and 0.816 ± 0.002 ($\mathrm{p\bar{p}}$). There is good agreement in JETSET for $\pi^{\pm}$ and $\mathrm{K}^{\pm}$, whereas the prediction for $\mathrm{p\bar{p}}$ is 2.0 standard deviations higher than the measured value. The discrepancy can be reduced using JETSET parameters [17] adjusted in order to describe the total Λ production rate. HERWIG overestimates the $\pi^{\pm}$ rate by about 2.0 standard deviations, whereas kaon and proton total rates are in better agreement with the data. However, the dependence of the cross section on the momentum is not well described.

The measured fractions of the three particle species as a function of momentum are shown in fig. 8 together with the JETSET and HERWIG Monte Carlo predictions. The errors shown have been derived as follows. In the counting method below 1.4 GeV/c there is no correlation of the particle rates within a particular momentum interval, whereas for high momenta full

correlation has been assumed. Again, for high momenta the $K^{\pm}$ fractions are underestimated by the Monte Carlo predictions and the $p\bar{p}$ fractions are overestimated.

The total fractions can be compared with data at lower centre of mass energies. Table 7 shows the total fractions measured by several experiments for $\sqrt{s} = 10$ GeV ([8, 9]) and (averaged by [29]) at about 29 GeV ([13, 10, 11, 12]), together with our data at 91.2 GeV. The total particle fractions for $\sqrt{s} = 29$ GeV and 91.2 GeV agree well within the errors. The fractional composition of pions, kaons and protons in events at these centre of mass energies does not change significantly.

Further insight into QCD calculations may be gained using the ξ distributions for individual particle types where $\xi = \ln(1/x_p)$ with $x_p = 2 \cdot p/\sqrt{s}$. Based on the modified leading log approximation (MLLA) [3] the shape of the ξ distribution for soft gluons is predicted, which can be directly compared to the observed hadron spectra under the assumption of local parton hadron duality (LPHD) [4].

The predicted hadron spectrum can be written as

$$\frac{1}{\sigma_{\mathrm{had}}} \frac{\mathrm{d}\sigma}{\mathrm{d}\xi} = N \cdot f\left(\Lambda_{\mathrm{eff}}, Q_0, \sqrt{s}, \xi\right) \quad , \tag{5}$$

where the effective QCD scale Λ_{eff} (which is not directly related to $\Lambda_{\overline{\mathrm{MS}}}$), the cut-off parameter Q_0 in the quark-gluon cascade, and the overall normalisation factor N are free parameters. A simplified form of this function is applied assuming $Q_0 = \Lambda_{\mathrm{eff}}$. Leaving Λ_{eff} as a free parameter, a higher Λ_{eff} has been obtained in data for higher particle masses [14, 16]. The ξ distribution is expected to be approximately Gaussian shaped with its peak shifted to lower values for more massive particles [30].

Fig. 9 shows the measured ξ distributions for pions, kaons and protons together with the interpolated functions used in fig. 7 drawn as solid lines. The hashed areas indicate the one standard deviation error under assumption of full correlation of the systematic errors as described before.

The peak positions of the ξ distributions for the individual particle species are obtained from the interpolated functions and are listed in table 8. The expected shift of the peak position is visible for kaons and protons with respect to pions. However, in contrast to the expectation from MLLA+LPHD [30], a smaller ξ peak value is observed for kaons than for protons. This fact becomes more evident by combining the obtained peak positions for charged pions, kaons and protons with other measurements.

In fig. 10 the peak positions of $\pi^{\pm}$, $K^{\pm}$ and $p\bar{p}$ are shown together with other data measured by the OPAL collaboration: K^0 [16], $K^*(892)^{\pm}$ [19], Λ, Ξ^- [17], as well as with data from the DELPHI collaboration: K^0,Λ [18] and the L3 collaboration: π^0 [14], η [15]. The figure clearly illustrates a mass dependence of the peak positions. However, the data in general do not strongly follow the MLLA+LPHD expectation of lower peak positions for higher masses. This is most evident for $K^*(892)^{\pm}$ and protons, indicating a step in the peak positions of mesons and baryons.

Fig. 10 also shows the predictions from the JETSET and HERWIG 5.0[4] Monte Carlo generators representing the string and the cluster fragmentation models. Both are in reasonable

[4]No significant differences are expected between HERWIG 5.0 and HERWIG 5.5

agreement with measured peak positions, the predictions using fragmentation models follow the observed step in the peak positions of mesons and baryons.

7 Summary

The cross sections of charged pions, kaons and protons as a function of x_E have been measured using 766 016 multihadronic Z^0 decays recorded with the OPAL detector. Using the energy loss measurement in the jet chamber, the momentum range up to the beam energy (45.6 GeV/c) has been covered, except for the cross-over regions of the energy loss functions. The yields were found to be 17.05 ± 0.43 $\pi^{\pm}$, 2.42 ± 0.13 $K^{\pm}$ and 0.92 ± 0.11 $p\bar{p}$ per multihadronic event with the statistical and systematic errors added in quadrature. The fractional composition of pions, kaons and protons does not change significantly compared to lower centre of mass energies of $\sqrt{s} = 10$ GeV and $\sqrt{s} = 29$ GeV.

The prediction of JETSET for the number of pions and kaons per multihadronic event (16.99 $\pi^{\pm}$, 2.26 $K^{\pm}$) agrees well with the data, whereas the predicted number of protons (1.15 $p\bar{p}$) is two standard deviations above the measured value. In contrast, the prediction of HERWIG for the kaons (2.47 $K^{\pm}$) and protons (0.82 $p\bar{p}$) are in agreement with the data, but the pion rate (17.75 $\pi^{\pm}$) is overestimated by two standard deviations.

The cross section as a function of x_E for pions ($\pi^{\pm}$) as predicted by JETSET is in good agreement with the data, whereas deviations are observed for kaons ($K^{\pm}$) and protons ($p\bar{p}$). The predictions by HERWIG at momenta less than 2.0 GeV/c show a significantly larger cross section for kaons, whereas the proton cross section is underestimated.

The cross sections as a function of $\xi = \ln(1/x_p)$ are approximately Gaussian shaped with the peak positions measured at $\xi_{\mathrm{peak}} = 3.81 \pm 0.02$ for pions, $\xi_{\mathrm{peak}} = 2.63 \pm 0.04$ for kaons and $\xi_{\mathrm{peak}} = 3.00 \pm 0.09$ for protons. Combining these data with other measurements there is evidence for a mass dependence that is different for mesons and baryons. Both JETSET and HERWIG 5.0 agree with the measured peak positions.

Acknowledgements:

It is a pleasure to thank the SL Division for the efficient operation of the LEP accelerator, the precise information on the absolute energy, and their continuing close cooperation with our experimental group. In addition to the support staff at our own institutions we are pleased to acknowledge the
Department of Energy, USA,
National Science Foundation, USA,
Texas National Research Laboratory Commission, USA,
Science and Engineering Research Council, UK,
Natural Sciences and Engineering Research Council, Canada,
Fussefeld Foundation,
Israeli Ministry of Energy and Ministry of Science,
Minerva Gesellschaft,
Japanese Ministry of Education, Science and Culture (the Monbusho) and a grant under the Monbusho International Science Research Program,
German Israeli Bi-national Science Foundation (GIF),
Direction des Sciences de la Matière du Commissariat à l'Energie Atomique, France,
Bundesministerium für Forschung und Technologie, Germany,
National Research Council of Canada,
A.P. Sloan Foundation and Junta Nacional de Investigação Científica e Tecnológica, Portugal.

References

[1] B. Andersson et al., Phys. Rep. **97** (1983) 31.

[2] G.C. Fox and S. Wolfram, Nucl. Phys. **B 168** (1980) 285;
S. Wolfram, 15th Rencontre de Moriond, Les Arcs (1980) 549.

[3] Y.I. Azimov, Y.L. Dokshitzer, V.A. Khoze and S.I. Troyan,
Zeit. f. Physik **C 27** (1985) 65.

[4] D. Amati and G. Veneziano, Phys. Lett. **B 83** (1979) 87;
Y.I. Azimov et al., Phys. Lett. **B 165** (1985) 147.

[5] T. Sjöstrand, Comp. Phys. Comm. **39** (1986) 347;
T. Sjöstrand and M. Bengtsson, Comp. Phys. Comm. **43** (1987) 367;
T. Sjöstrand, CERN-TH.6488/92.

[6] G. Marchesini and B. Webber, Nucl. Phys. **B 310** (1988) 461;
G. Marchesini et al., Comp. Phys. Comm. **67** (1992) 465.

[7] OPAL Collab., M. Z. Akrawy et al., Zeit. f. Physik **C 47** (1990) 505.

[8] CLEO Collab., S. Behrends et al., Phys. Rev. **D 31** (1985) 2161.

[9] ARGUS Collab., H. Albrecht et al., Zeit. f. Physik **C 39** (1988) 177.

[10] TASSO Collab., M. Althoff et al., Zeit. f. Physik **C 17** (1983) 5.

[11] TPC Collab., H. Aihara et al., Phys. Rev. Lett. **52** (1984) 577;
TPC Collab., H. Aihara et al., Phys. Rev. Lett. **61** (1988) 1263.

[12] Mark II Collab., H. Schellman et al., Phys. Rev. **D 31** (1985) 3013.

[13] HRS Collab., M. Derrick et al., Phys. Rev. **D 35** (1987) 2639.

[14] L3 Collab., B. Adeva et al., Phys. Lett. **B 259** (1991) 199.

[15] L3 Collab., O. Adriani et al., Phys. Lett. **B 286** (1992) 403.

[16] OPAL Collab., G. Alexander et al., Phys. Lett. **B 264** (1991) 467.

[17] OPAL Collab., P. Acton et al., Phys. Lett. **B 291** (1992) 503.

[18] DELPHI Collab., P. Abreu et al., Phys. Lett. **B 275** (1992) 231;
DELPHI Collab., P. Abreu et al., Phys. Lett. **B 318** (1993) 249.

[19] OPAL Collab., P. Acton et al., Phys. Lett. **B 305** (1993) 407.

[20] OPAL Collab., K. Ahmet et al., Nucl. Instr. and Meth. **A 305** (1991) 275.

[21] M. Hauschild et al., Nucl. Instr. and Meth. **A 314** (1992) 74.

[22] OPAL Collab., G. Alexander et al., Zeit. f. Physik **C 52** (1991) 175.

[23] H.A. Bethe, Handbuch der Physik **24/1** (Springer, Berlin, 1933) 491.

[24] See for example: D. Jeanne et al., Nucl. Instr. and Meth. **111** (1973) 287.

[25] J. Allison et al., Nucl. Instr. and Meth. **A 317** (1992) 47.

[26] R.M. Sternheimer and R.F. Peierls, Phys. Rev. **B 3** (1971) 3681.

[27] OPAL Collab., P. Acton et al., Zeit. f. Physik **C 58** (1993) 523.

[28] OPAL Collab., P. Acton et al., Zeit. f. Physik **C 53** (1992) 539.

[29] W. Hofmann, Ann. Rev. Nucl. Part. Sci. **38** (1988) 279.

[30] Y.L. Dokshitzer, V.A. Khoze and S.I. Troyan,
J. Phys. G: Nucl. Part. Phys. **17** (1991) 1481;
Y.L. Dokshitzer, V.A. Khoze and S.I. Troyan,
Zeit. f. Physik **C 55** (1992) 107.

Tables

p in GeV/c	g_c	g_m	g_σ
0.15	0.051	0.25	1.74
0.31	0.046	0.25	1.78
0.51	0.047	0.23	1.79
1.02	0.051	0.17	1.82
3.08	0.061	0.08	1.86
5.47	0.064	0.06	1.86
9.95	0.062	0.06	1.85
18.08	0.057	0.10	1.84
23.80	0.055	0.14	1.82

Table 1: Typical double Gaussian parameters. See text for details.

	$p < 1.4$ GeV/c counting method			$p > 2.0$ GeV/c fitting method		
Source of error	pions	kaons	protons	pions	kaons	protons
track cuts	0.2	2.2	3.4	0.6	1.0	5.4
muon subtraction	0.5	0.0	0.0	0.5	0.0	0.0
momentum correction	0.5	1.0	2.0	0.5	0.5	0.5
nuclear interaction	2.8	0.6	1.0	-	-	-
decay in flight	0.2	0.2	0.0	-	-	-
fit method	-	-	-	1.4	2.9	9.6
relative resolution	-	-	-	1.0	5.0	5.0
double Gaussian	-	-	-	0.7	1.6	9.9
start values	-	-	-	2.1	0.4	1.8
total	2.9	2.5	4.1	3.0	6.1	15.7

Table 2: Systematic errors for the differential cross sections in %. Only mean values are given, the actual values differ for individual momentum intervals. See text for more details.

p	$\langle p \rangle$	$\pi^{\pm}$-rates $\pm \Delta_{\mathrm{stat}} \pm \Delta_{\mathrm{sys}}$
0.227-0.239	0.233	9.89 $\pm$ 0.07 $\pm$ 0.29
0.239-0.251	0.245	9.98 $\pm$ 0.07 $\pm$ 0.29
0.251-0.263	0.257	10.37 $\pm$ 0.07 $\pm$ 0.31
0.263-0.276	0.270	10.38 $\pm$ 0.07 $\pm$ 0.31
0.276-0.290	0.283	10.42 $\pm$ 0.07 $\pm$ 0.31
0.290-0.305	0.298	10.40 $\pm$ 0.07 $\pm$ 0.31
0.305-0.320	0.313	10.53 $\pm$ 0.06 $\pm$ 0.31
0.320-0.336	0.328	10.66 $\pm$ 0.06 $\pm$ 0.31
0.336-0.353	0.345	10.53 $\pm$ 0.06 $\pm$ 0.31
0.353-0.371	0.362	10.56 $\pm$ 0.06 $\pm$ 0.31
0.371-0.390	0.381	10.46 $\pm$ 0.06 $\pm$ 0.31
0.390-0.410	0.400	10.23 $\pm$ 0.06 $\pm$ 0.30
0.410-0.431	0.420	10.29 $\pm$ 0.06 $\pm$ 0.30
0.431-0.453	0.442	10.02 $\pm$ 0.05 $\pm$ 0.29
0.453-0.476	0.464	9.83 $\pm$ 0.05 $\pm$ 0.29
0.476-0.500	0.488	9.62 $\pm$ 0.05 $\pm$ 0.28
0.500-0.525	0.513	9.46 $\pm$ 0.05 $\pm$ 0.28
0.525-0.552	0.539	9.23 $\pm$ 0.05 $\pm$ 0.27
0.552-0.580	0.566	9.05 $\pm$ 0.05 $\pm$ 0.26
0.580-0.610	0.595	8.71 $\pm$ 0.04 $\pm$ 0.25
0.610-0.641	0.625	8.40 $\pm$ 0.04 $\pm$ 0.25
0.641-0.673	0.657	8.12 $\pm$ 0.04 $\pm$ 0.24
0.673-0.708	0.691	7.87 $\pm$ 0.04 $\pm$ 0.23
0.708-0.744	0.726	7.50 $\pm$ 0.04 $\pm$ 0.22
0.744-0.782	0.763	7.26 $\pm$ 0.03 $\pm$ 0.21
0.782-0.822	0.802	6.95 $\pm$ 0.03 $\pm$ 0.20
0.822-0.864	0.843	6.56 $\pm$ 0.04 $\pm$ 0.20
2.02- 2.12	2.07	2.374 $\pm$ 0.031 $\pm$ 0.209
2.12- 2.23	2.17	2.264 $\pm$ 0.013 $\pm$ 0.079
2.23- 2.34	2.28	2.103 $\pm$ 0.018 $\pm$ 0.036
2.34- 2.46	2.40	1.944 $\pm$ 0.010 $\pm$ 0.027
2.46- 2.59	2.52	1.793 $\pm$ 0.008 $\pm$ 0.026
2.59- 2.72	2.65	1.672 $\pm$ 0.009 $\pm$ 0.024
2.72- 2.86	2.79	1.550 $\pm$ 0.013 $\pm$ 0.024
2.86- 3.01	2.93	1.420 $\pm$ 0.008 $\pm$ 0.022
3.01- 3.16	3.08	1.328 $\pm$ 0.008 $\pm$ 0.019
3.16- 3.32	3.24	1.221 $\pm$ 0.008 $\pm$ 0.017
3.32- 3.49	3.41	1.115 $\pm$ 0.007 $\pm$ 0.015
3.49- 3.67	3.58	1.035 $\pm$ 0.007 $\pm$ 0.015
3.67- 3.86	3.76	0.955 $\pm$ 0.006 $\pm$ 0.014
3.86- 4.06	3.96	0.879 $\pm$ 0.006 $\pm$ 0.012
4.06- 4.95	4.48	0.705 $\pm$ 0.003 $\pm$ 0.009
4.95- 6.05	5.47	0.478 $\pm$ 0.002 $\pm$ 0.007
6.05- 7.39	6.68	0.319 $\pm$ 0.001 $\pm$ 0.005
7.39- 9.02	8.15	0.2052 $\pm$ 0.0012 $\pm$ 0.0032
9.02-11.02	9.95	0.1246 $\pm$ 0.0008 $\pm$ 0.0024
11.02-13.46	12.14	0.0717 $\pm$ 0.0006 $\pm$ 0.0016
13.46-16.44	14.82	0.0386 $\pm$ 0.0005 $\pm$ 0.0012
16.44-20.08	18.08	0.0206 $\pm$ 0.0004 $\pm$ 0.0013
20.08-29.95	23.81	0.0058 $\pm$ 0.0001 $\pm$ 0.0004
29.95-45.60	33.97	0.0006 $\pm$ 0.0001 $\pm$ 0.0002

Table 3: Momentum dependent cross section for charged pions ($\pi^{\pm}$). Rates in units of $\frac{1}{\sigma_{\mathrm{had}}} \cdot \frac{\mathrm{d}\sigma}{\mathrm{d}p}$ $[(\frac{\mathrm{GeV}}{c})^{-1}]$.

p	$\langle p \rangle$	$K^{\pm}$-rates $\pm \Delta_{stat} \pm \Delta_{sys}$
0.271-0.281	0.276	0.363 $\pm$ 0.030 $\pm$ 0.028
0.281-0.292	0.287	0.373 $\pm$ 0.027 $\pm$ 0.028
0.292-0.304	0.298	0.367 $\pm$ 0.024 $\pm$ 0.025
0.304-0.317	0.311	0.374 $\pm$ 0.022 $\pm$ 0.023
0.317-0.331	0.324	0.375 $\pm$ 0.021 $\pm$ 0.019
0.331-0.346	0.339	0.410 $\pm$ 0.020 $\pm$ 0.019
0.346-0.362	0.354	0.431 $\pm$ 0.020 $\pm$ 0.019
0.362-0.379	0.371	0.418 $\pm$ 0.018 $\pm$ 0.020
0.379-0.397	0.388	0.456 $\pm$ 0.018 $\pm$ 0.016
0.397-0.416	0.406	0.499 $\pm$ 0.018 $\pm$ 0.017
0.416-0.436	0.426	0.514 $\pm$ 0.017 $\pm$ 0.016
0.436-0.457	0.447	0.486 $\pm$ 0.011 $\pm$ 0.011
0.457-0.480	0.469	0.522 $\pm$ 0.011 $\pm$ 0.011
0.480-0.504	0.492	0.541 $\pm$ 0.011 $\pm$ 0.012
0.504-0.528	0.516	0.539 $\pm$ 0.011 $\pm$ 0.018
0.528-0.555	0.542	0.557 $\pm$ 0.011 $\pm$ 0.020
0.555-0.583	0.569	0.587 $\pm$ 0.011 $\pm$ 0.014
0.583-0.612	0.597	0.590 $\pm$ 0.010 $\pm$ 0.048
0.612-0.643	0.627	0.586 $\pm$ 0.010 $\pm$ 0.016
0.643-0.675	0.659	0.591 $\pm$ 0.010 $\pm$ 0.044
0.675-0.709	0.692	0.614 $\pm$ 0.009 $\pm$ 0.024
0.709-0.745	0.727	0.597 $\pm$ 0.009 $\pm$ 0.025
0.745-0.783	0.764	0.613 $\pm$ 0.009 $\pm$ 0.031
4.05- 4.95	4.48	0.181 $\pm$ 0.004 $\pm$ 0.015
4.95- 6.05	5.46	0.138 $\pm$ 0.003 $\pm$ 0.009
6.05- 7.38	6.67	0.103 $\pm$ 0.001 $\pm$ 0.006
7.38- 9.02	8.15	0.0767 $\pm$ 0.0010 $\pm$ 0.0042
9.02-11.01	9.94	0.0536 $\pm$ 0.0006 $\pm$ 0.0029
11.01-13.45	12.13	0.0349 $\pm$ 0.0005 $\pm$ 0.0018
13.45-16.43	14.81	0.0220 $\pm$ 0.0003 $\pm$ 0.0012
16.43-20.06	18.07	0.0127 $\pm$ 0.0003 $\pm$ 0.0007
20.06-29.93	23.79	0.0042 $\pm$ 0.0001 $\pm$ 0.0003
29.93-45.60	33.94	0.0004 $\pm$ 0.0001 $\pm$ 0.0001

Table 4: Momentum dependent cross section for charged kaons ($K^{\pm}$). Rates in units of $\frac{1}{\sigma_{had}} \cdot \frac{d\sigma}{dp}$ $[(\frac{GeV}{c})^{-1}]$.

p	$\langle p \rangle$	$\mathrm{p\bar{p}}$-rates $\pm \Delta_{\mathrm{stat}} \pm \Delta_{\mathrm{sys}}$		
0.406-0.421	0.414	0.169	$\pm$ 0.010	$\pm$ 0.013
0.421-0.438	0.429	0.174	$\pm$ 0.009	$\pm$ 0.015
0.438-0.456	0.447	0.171	$\pm$ 0.009	$\pm$ 0.012
0.456-0.475	0.465	0.185	$\pm$ 0.008	$\pm$ 0.015
0.475-0.495	0.485	0.181	$\pm$ 0.008	$\pm$ 0.006
0.495-0.517	0.506	0.202	$\pm$ 0.008	$\pm$ 0.010
0.517-0.541	0.529	0.215	$\pm$ 0.008	$\pm$ 0.012
0.541-0.565	0.553	0.228	$\pm$ 0.008	$\pm$ 0.014
0.565-0.592	0.579	0.230	$\pm$ 0.008	$\pm$ 0.010
0.592-0.620	0.606	0.230	$\pm$ 0.008	$\pm$ 0.007
0.620-0.650	0.635	0.236	$\pm$ 0.007	$\pm$ 0.012
0.650-0.681	0.665	0.239	$\pm$ 0.007	$\pm$ 0.008
0.681-0.714	0.698	0.246	$\pm$ 0.007	$\pm$ 0.006
0.714-0.750	0.732	0.248	$\pm$ 0.007	$\pm$ 0.009
0.750-0.787	0.768	0.248	$\pm$ 0.004	$\pm$ 0.009
0.787-0.826	0.806	0.254	$\pm$ 0.004	$\pm$ 0.008
0.826-0.867	0.846	0.260	$\pm$ 0.004	$\pm$ 0.007
0.867-0.911	0.889	0.260	$\pm$ 0.004	$\pm$ 0.007
0.911-0.957	0.933	0.257	$\pm$ 0.004	$\pm$ 0.006
0.957-1.005	0.980	0.263	$\pm$ 0.004	$\pm$ 0.007
1.005-1.056	1.030	0.257	$\pm$ 0.004	$\pm$ 0.021
1.056-1.109	1.082	0.256	$\pm$ 0.004	$\pm$ 0.027
1.109-1.166	1.137	0.257	$\pm$ 0.004	$\pm$ 0.029
1.166-1.225	1.195	0.248	$\pm$ 0.004	$\pm$ 0.027
1.225-1.287	1.256	0.241	$\pm$ 0.004	$\pm$ 0.017
1.287-1.353	1.320	0.250	$\pm$ 0.004	$\pm$ 0.016
1.353-1.422	1.387	0.245	$\pm$ 0.004	$\pm$ 0.021
4.05- 4.95	4.47	0.0606	$\pm$ 0.0036	$\pm$ 0.0129
4.95- 6.04	5.46	0.0517	$\pm$ 0.0029	$\pm$ 0.0062
6.04- 7.38	6.67	0.0352	$\pm$ 0.0011	$\pm$ 0.0031
7.38- 9.01	8.14	0.0214	$\pm$ 0.0011	$\pm$ 0.0023
9.01-11.01	9.94	0.0152	$\pm$ 0.0006	$\pm$ 0.0021
11.01-13.44	12.12	0.0093	$\pm$ 0.0004	$\pm$ 0.0013
13.44-16.42	14.80	0.0045	$\pm$ 0.0003	$\pm$ 0.0006
16.42-20.05	18.05	0.0015	$\pm$ 0.0002	$\pm$ 0.0005
20.05-29.90	23.78	0.00056	$\pm$ 0.00005	$\pm$ 0.00014
29.90-45.60	33.92	0.000015	$\pm$ 0.000004	$\pm$ 0.000026

Table 5: Momentum dependent cross section for protons ($\mathrm{p\bar{p}}$). Rates in units of $\frac{1}{\sigma_{\mathrm{had}}} \cdot \frac{\mathrm{d}\sigma}{\mathrm{d}p}\ [(\frac{\mathrm{GeV}}{c})^{-1}]$.

source of rates	pions ($\pi^{\pm}$)	kaons ($\mathrm{K}^{\pm}$)	protons ($\mathrm{p\bar{p}}$)
extrapolation MC	1.166 $\pm$ 0.023	0.034 $\pm$ 0.002	0.024 $\pm$ 0.005
data low p	5.684 $\pm$ 0.170	0.270 $\pm$ 0.014	0.245 $\pm$ 0.016
interpolation data	4.638 $\pm$ 0.112	1.188 $\pm$ 0.057	0.376 $\pm$ 0.049
data high p	5.564 $\pm$ 0.124	0.929 $\pm$ 0.060	0.270 $\pm$ 0.041
total data	17.052 $\pm$ 0.429	2.421 $\pm$ 0.133	0.916 $\pm$ 0.111
total JETSET 7.3	16.992 $\pm$ 0.005	2.258 $\pm$ 0.002	1.145 $\pm$ 0.001
total HERWIG 5.5	17.754 $\pm$ 0.008	2.471 $\pm$ 0.003	0.816 $\pm$ 0.002

Table 6: Total rates per event for pions, kaons and protons.

$\sqrt{s}$	pions ($\pi^{\pm}$)	kaons ($K^{\pm}$)	protons ($p\bar{p}$)
10.0 GeV	84.0% ± 1.9%	13.2% ± 1.8%	2.8% ± 0.7%
29.0 GeV	83.3% ± 0.9%	12.0% ± 0.8%	4.7% ± 0.4%
91.2 GeV	83.6% ± 0.8%	11.9% ± 0.6%	4.5% ± 0.5%

Table 7: Total fraction for pions, kaons and protons in % compared with data from lower centre of mass energies.

particle species	ξ_{peak}
pions ($\pi^{\pm}$)	3.81 ± 0.02
kaons ($K^{\pm}$)	2.63 ± 0.04
protons ($p\bar{p}$)	3.00 ± 0.09

Table 8: Peak position ξ_{peak} of the $\xi = \ln(1/x_p)$ distributions for pions, kaons and protons.

Figure Captions

Figure 1: Truncated mean energy loss $\mathrm{d}E/\mathrm{d}x$ for tracks in multihadronic events as a function of the particle momentum. The two indicated slices represent the momentum intervals of figs. 3a and 3b.

Figure 2: Two particle separation power $(\mathrm{d}E/\mathrm{d}x_1 - \mathrm{d}E/\mathrm{d}x_2)/\langle\sigma(\mathrm{d}E/\mathrm{d}x)\rangle$ in units of mean $\mathrm{d}E/\mathrm{d}x$ resolution $\langle\sigma(\mathrm{d}E/\mathrm{d}x)\rangle = \sqrt{\sigma(\mathrm{d}E/\mathrm{d}x_1)^2 + \sigma(\mathrm{d}E/\mathrm{d}x_2)^2}$ as a function of particle momentum for tracks with at least 100 measured samples obtained from data. The curves given are for electron/pion, pion/kaon and kaon/proton separation.

Figure 3: Truncated mean energy loss $\mathrm{d}E/\mathrm{d}x$ for tracks in multihadronic events in the momentum intervals 0.45–0.48 GeV/c (a) and 11.0–13.5 GeV/c (b). The curves shown in (b) represent the results of the simultaneous double Gaussian fit as described in the text. The double Gaussian structure is visible due to the logarithmic scale chosen in (a) and (b) as well as the minor overlap between the different particle species in (a). In (a), the inset shows the same plot with a linear scale on the ordinate.

Figure 4: Deposited charge distribution Q_{dep} for the momentum intervals 0.45–0.48 GeV/c (a) and 11.0–13.5 GeV/c (b). Reweighted sum of single distributions for the momentum intervals 0.45–0.48 GeV/c (c) and 11.0–13.5 GeV/c (d) with double Gaussian fits (full lines). The dashed and the dotted lines indicate the narrow and the broad Gaussians, respectively. See text for details.

Figure 5: Normalised $\mathrm{d}E/\mathrm{d}x$ distribution $(\mathrm{d}E/\mathrm{d}x_{\mathrm{measured}} - \mathrm{d}E/\mathrm{d}x_{\mathrm{expected}})/\sigma(\mathrm{d}E/\mathrm{d}x)$ of pions from $\mathrm{K}^0_{\mathrm{S}} \to \pi^+\pi^-$ decays with a momentum $p > 2.0$ GeV/c where $\sigma(\mathrm{d}E/\mathrm{d}x)$ is the $\mathrm{d}E/\mathrm{d}x$ error obtained from eqs. 1 and 2. The curve shown represents the result of a single Gaussian fit with a central value of -0.112σ and a width of 0.997σ.

Figure 6: Differential cross sections for pions (a), kaons (b) and protons (c) as a function of momentum p for data (points), JETSET 7.3 (full line) and HERWIG 5.5 (dotted line) and ratios of data and predictions. The errors given are statistical and systematic errors added in quadrature.

Figure 7: Differential cross sections as a function of x_E for pions (a), kaons (b) and protons (c) for data (points), JETSET 7.3 (full line) and HERWIG 5.5 (dotted line). The errors given are statistical and systematic errors added in quadrature. The dashed line indicates the fitted function used for interpolation of the cross-over regions. For pions (a) this function is indistinguishable from the JETSET 7.3 curve.

Figure 8: Fractions of charged hadrons (pions, kaons and protons) as a function of the particle momentum p for data (points), JETSET 7.3 (line) and HERWIG 5.5 (dotted line). The errors given are statistical and systematic error added in quadrature. The dashed lines indicate the fitted functions used for interpolation of the cross-over regions.

Figure 9: Differential cross sections as a function of $\xi = \ln(1/x_p)$ for pions (a), kaons (b) and protons (c). The errors given are statistical and systematic errors added in quadrature. The solid lines are taken from the fitted functions used for interpolation of the cross-over regions as function of x_E. The hashed areas indicate the one standard deviation error under assumption of full correlation of the systematic errors as described in the text.

Figure 10: Measured peak positions ξ_{peak} of the ξ distributions for various particle species as function of the particle masses. The particles are grouped into mesons and baryons. Predictions from JETSET 7.3 (line) and HERWIG 5.0 (dotted line) are also shown.

Fig. 1

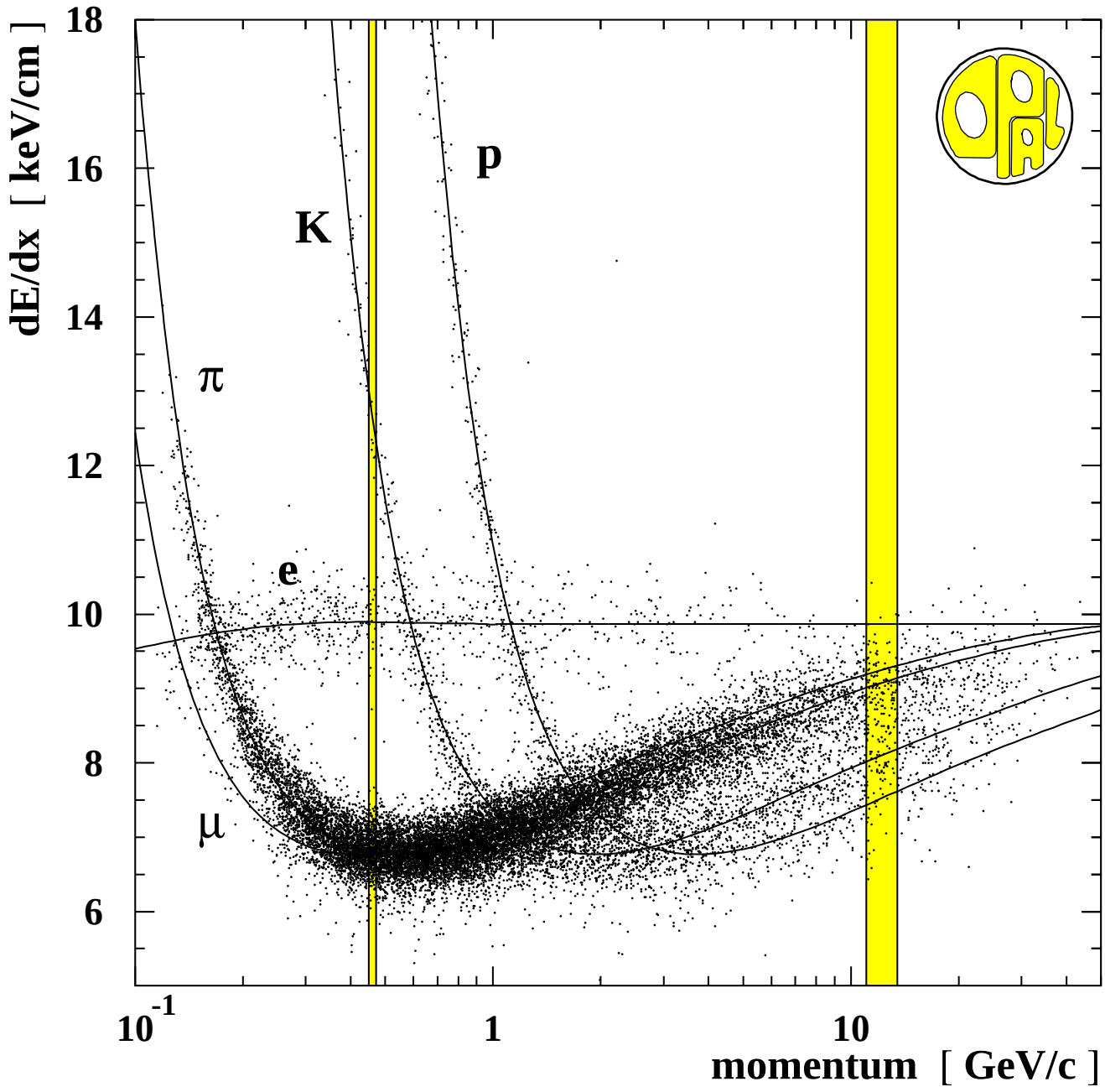

Fig. 2

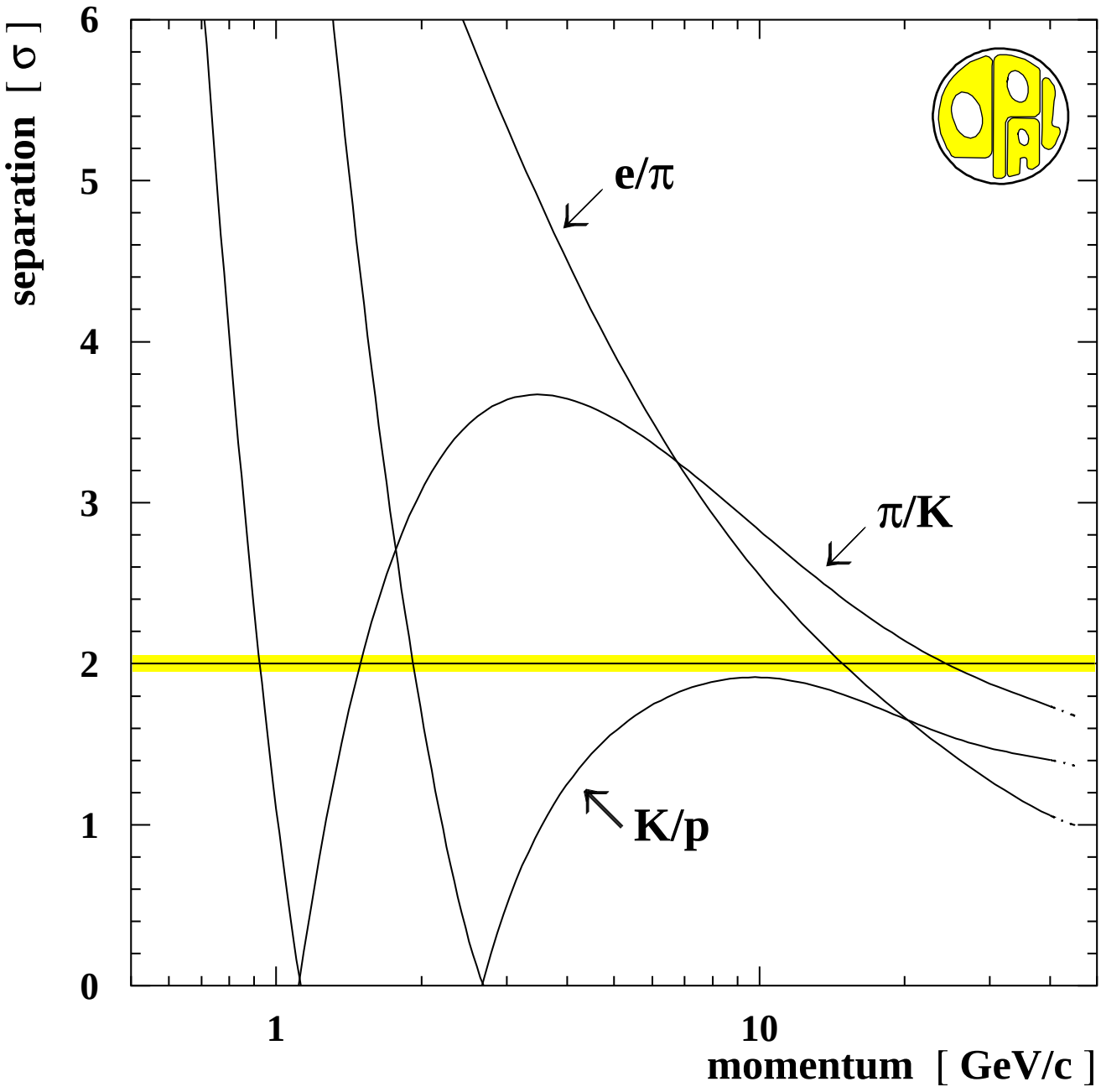

Fig. 3a

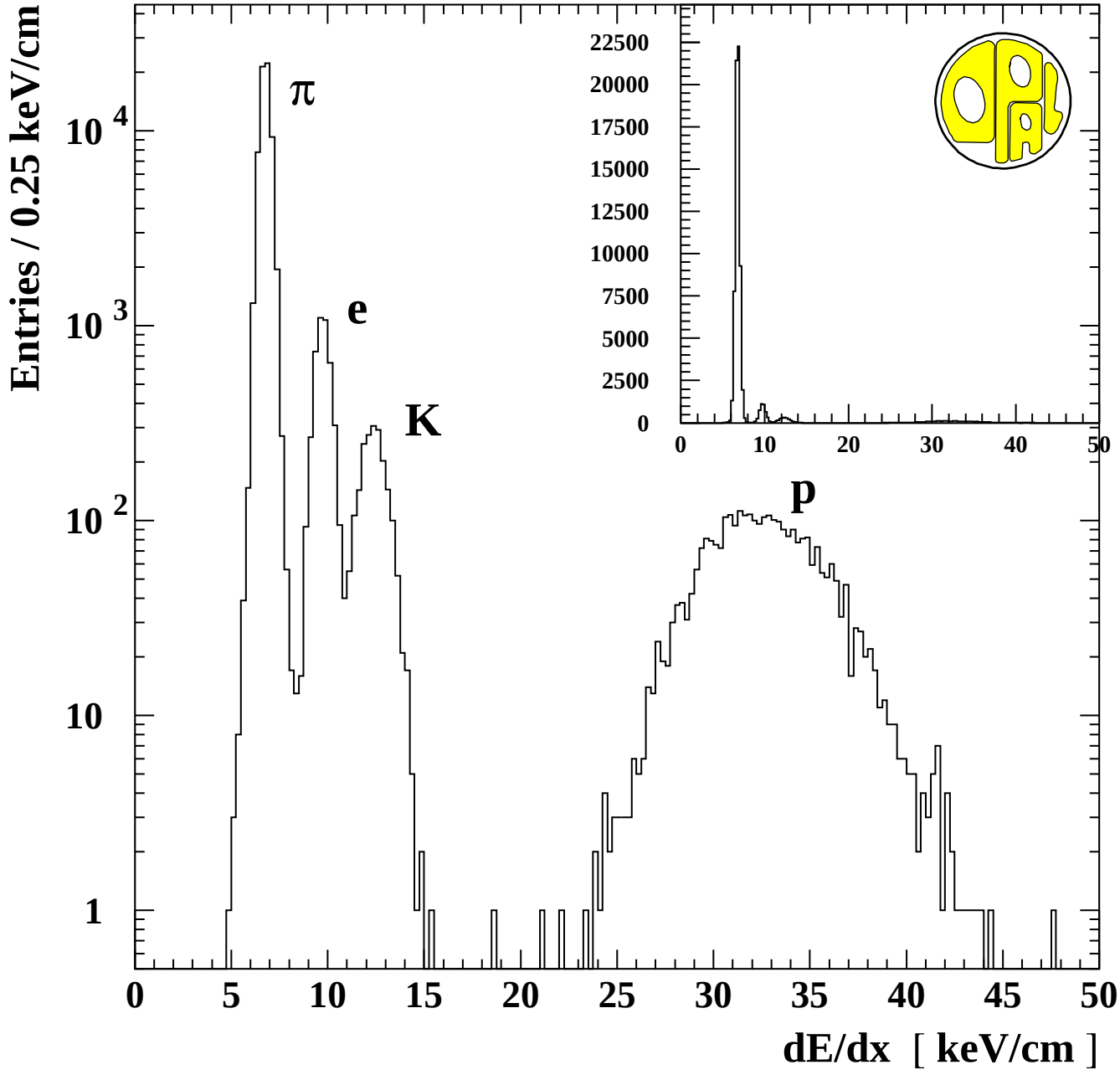
Entries / 0.25 keV/cm
10 4
10 3
10 2
10
1
π
e
K
p
0
5
10
15
20
25
30
35
40
45
50
dE/dx [keV/cm]
22500
20000
17500
15000
12500
10000
7500
5000
2500
0
0
10
20
30
40
50

Fig. 3b

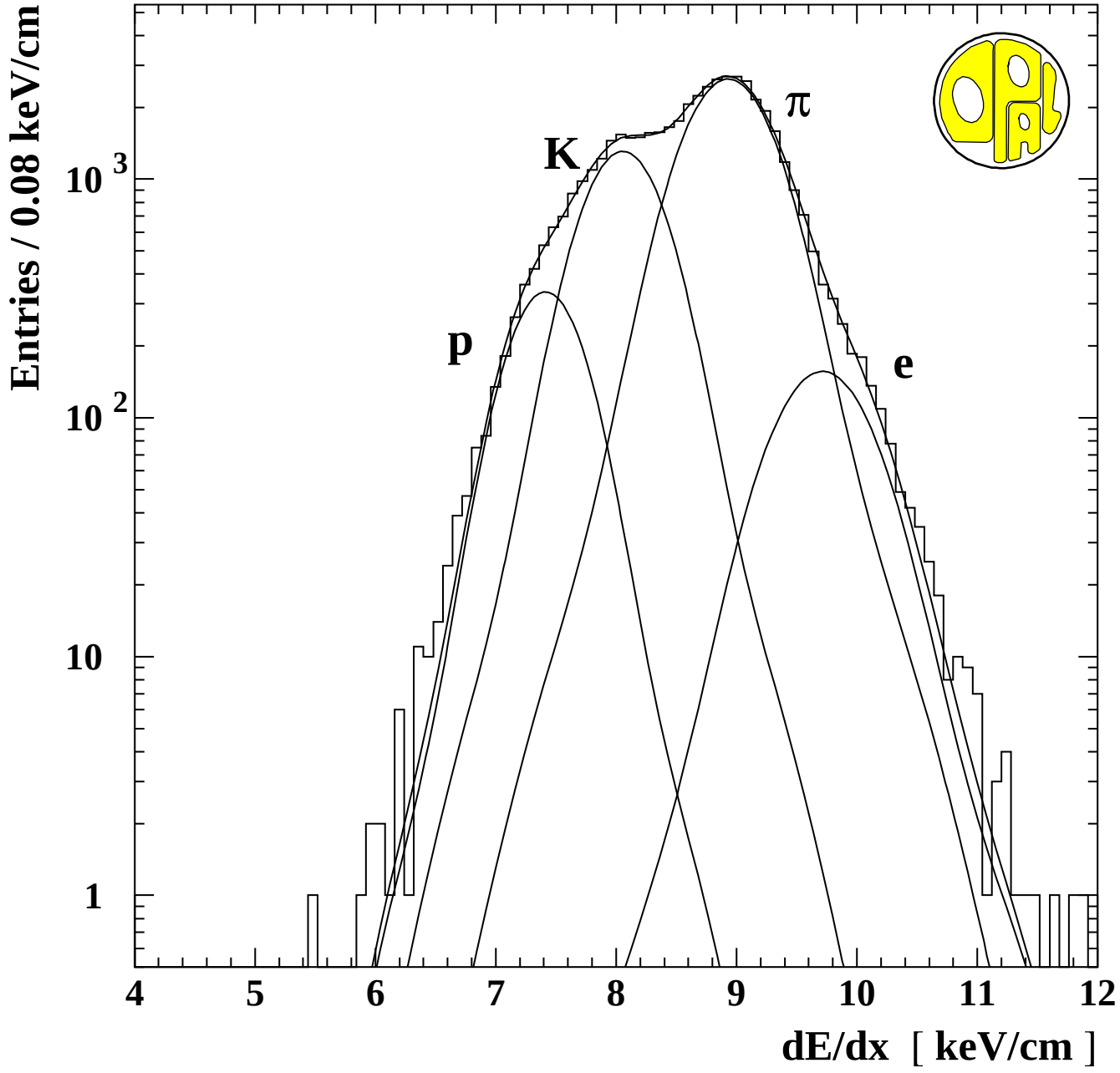

Fig. 4

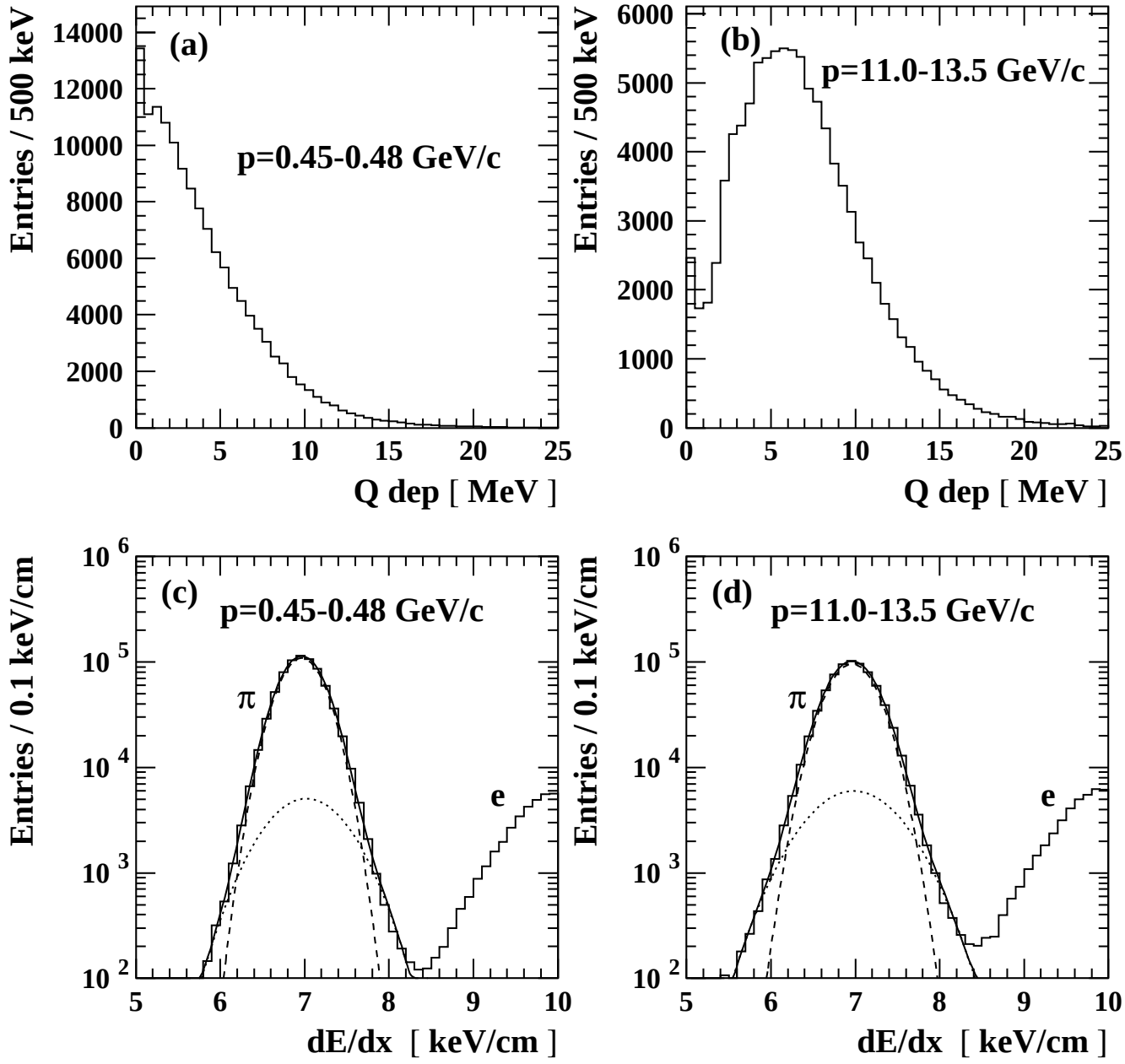
(a)
p=0.45-0.48 GeV/c
Entries / 500 keV
Q dep [MeV]
(b)
p=11.0-13.5 GeV/c
Entries / 500 keV
Q dep [MeV]
(c)
p=0.45-0.48 GeV/c
π
e
Entries / 0.1 keV/cm
dE/dx [keV/cm]
(d)
p=11.0-13.5 GeV/c
π
e
Entries / 0.1 keV/cm
dE/dx [keV/cm]

Fig. 5

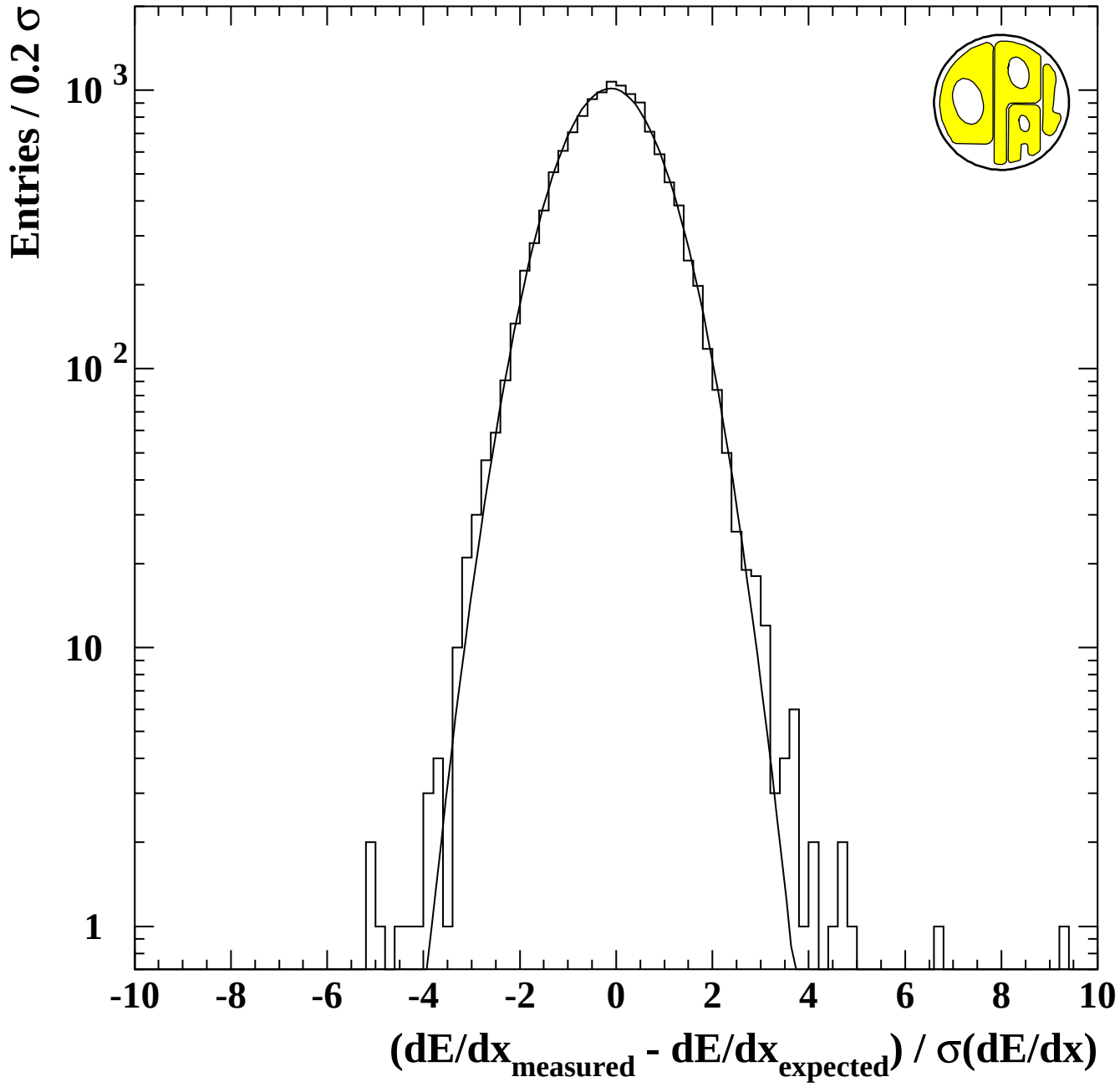
Entries / 0.2 σ
10 3
10 2
10
1
-10
-8
-6
-4
-2
0
2
4
6
8
10
(dE/dx measured - dE/dx expected) / σ(dE/dx)

Fig. 6a

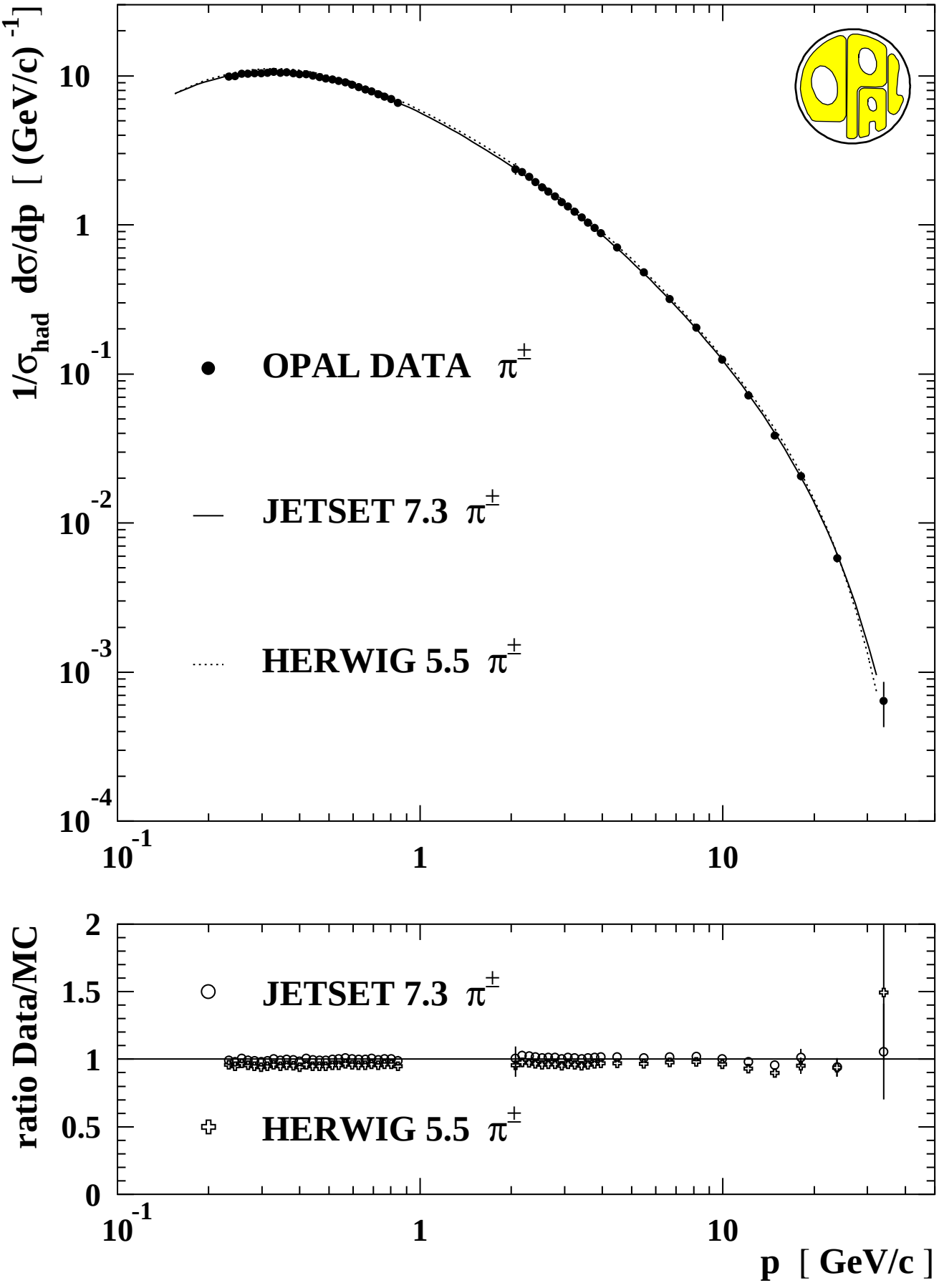
1/σ_had dσ/dp [(GeV/c)^-1]
OPAL DATA π±
JETSET 7.3 π±
HERWIG 5.5 π±
ratio Data/MC
JETSET 7.3 π±
HERWIG 5.5 π±
p [GeV/c]

Fig. 6b

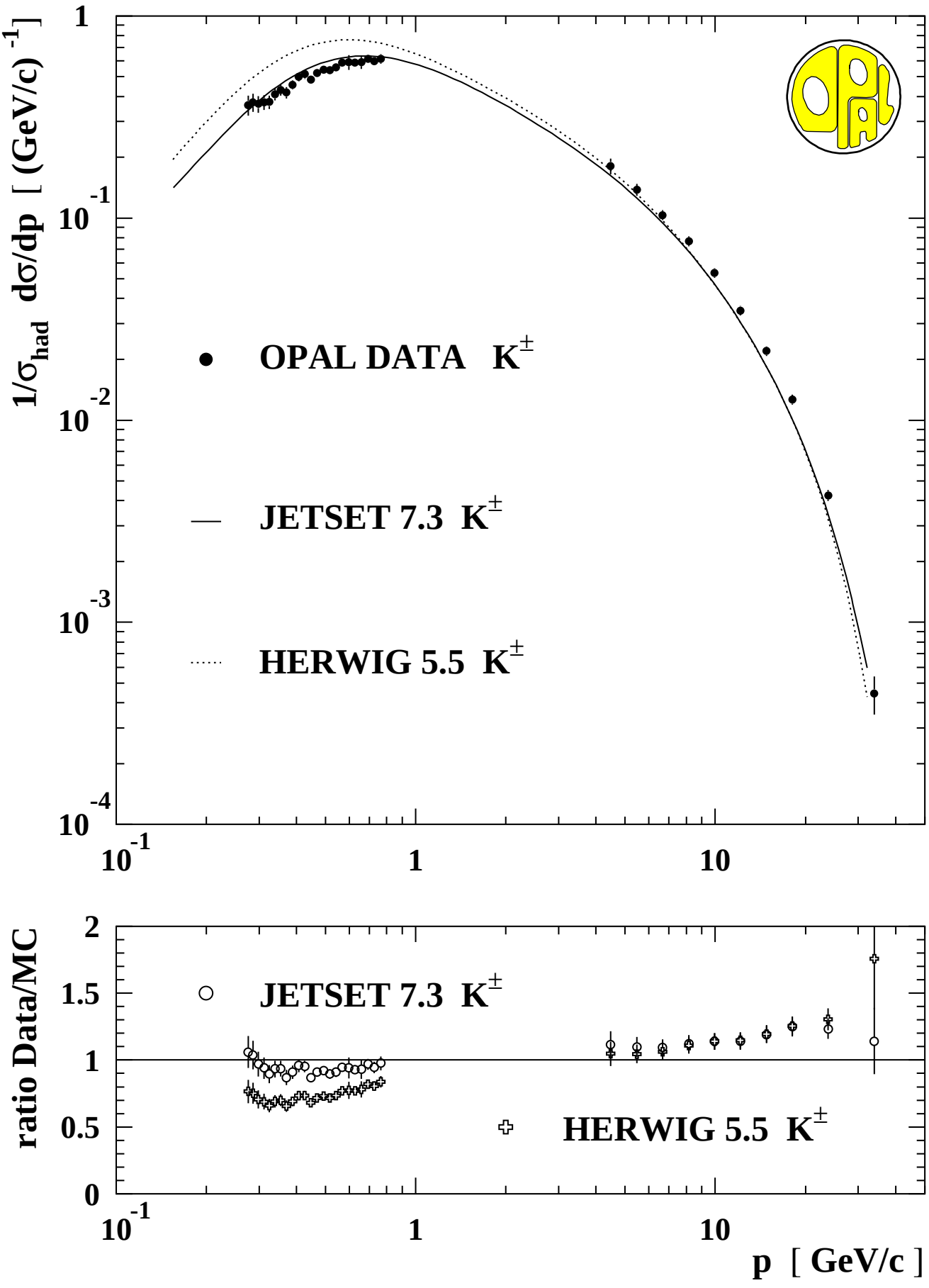
1/σ_had dσ/dp [(GeV/c)^-1]
OPAL DATA K±
JETSET 7.3 K±
HERWIG 5.5 K±
ratio Data/MC
JETSET 7.3 K±
HERWIG 5.5 K±
p [GeV/c]

Fig. 6c

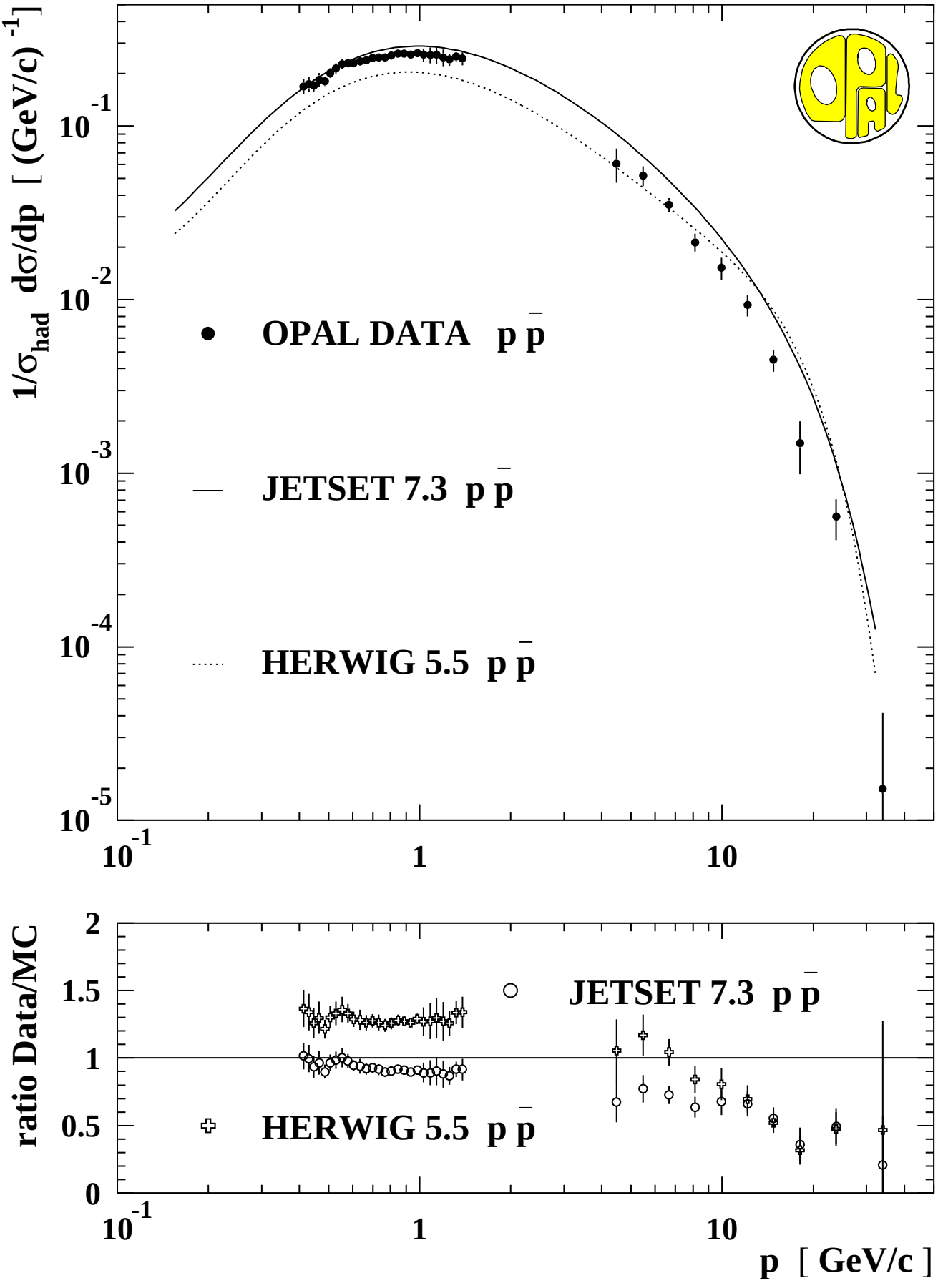
1/σ_had dσ/dp [(GeV/c)^-1]
OPAL DATA p p̄
JETSET 7.3 p p̄
HERWIG 5.5 p p̄
ratio Data/MC
JETSET 7.3 p p̄
HERWIG 5.5 p p̄
p [GeV/c]

Fig. 7a

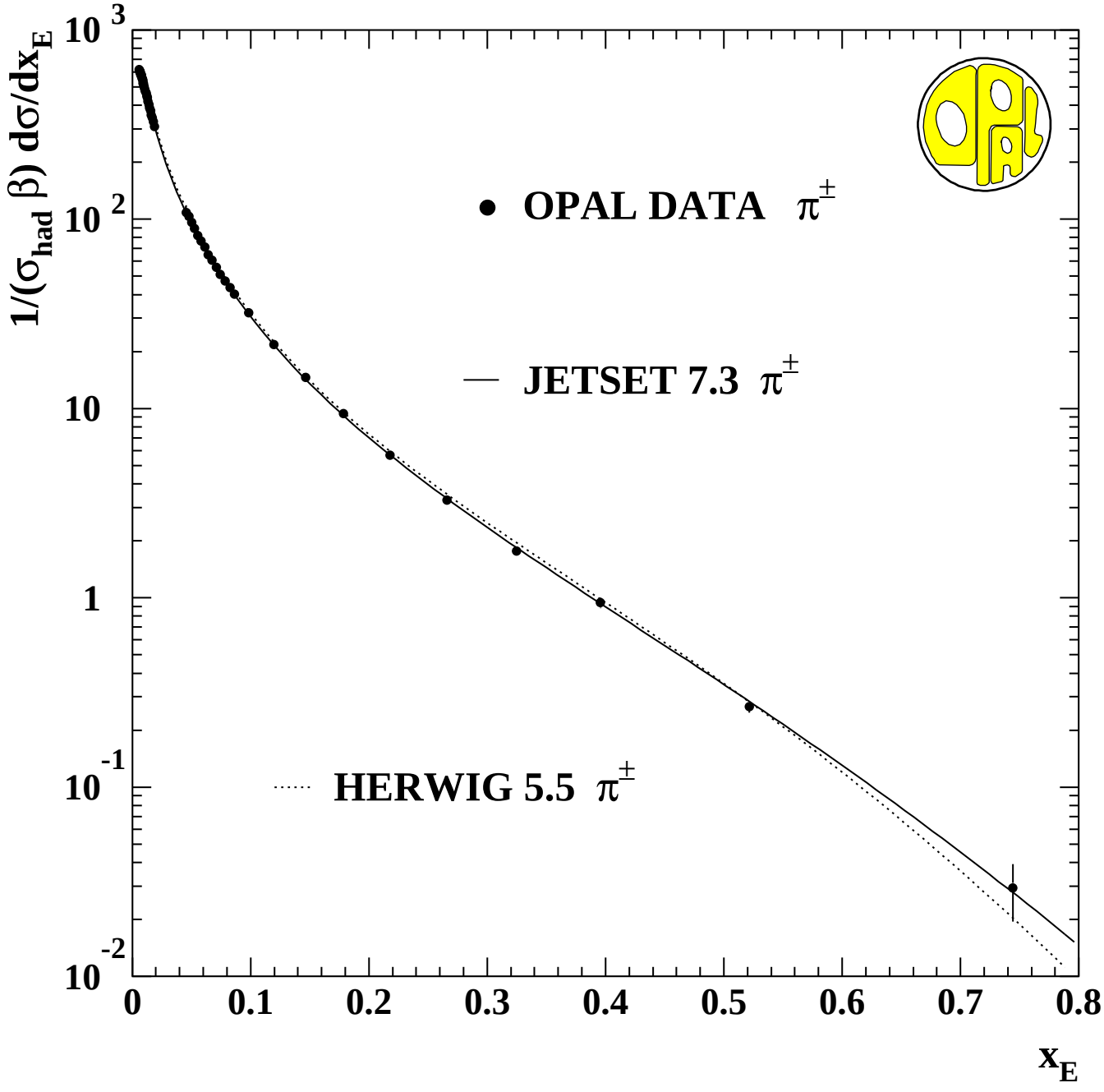
$1/(\sigma_{had}\,\beta)\ d\sigma/dx_E$
10^3
10^2
10
1
10^{-1}
10^{-2}
0
0.1
0.2
0.3
0.4
0.5
0.6
0.7
0.8
x_E
OPAL DATA $\pi^{\pm}$
JETSET 7.3 $\pi^{\pm}$
HERWIG 5.5 $\pi^{\pm}$

Fig. 7b

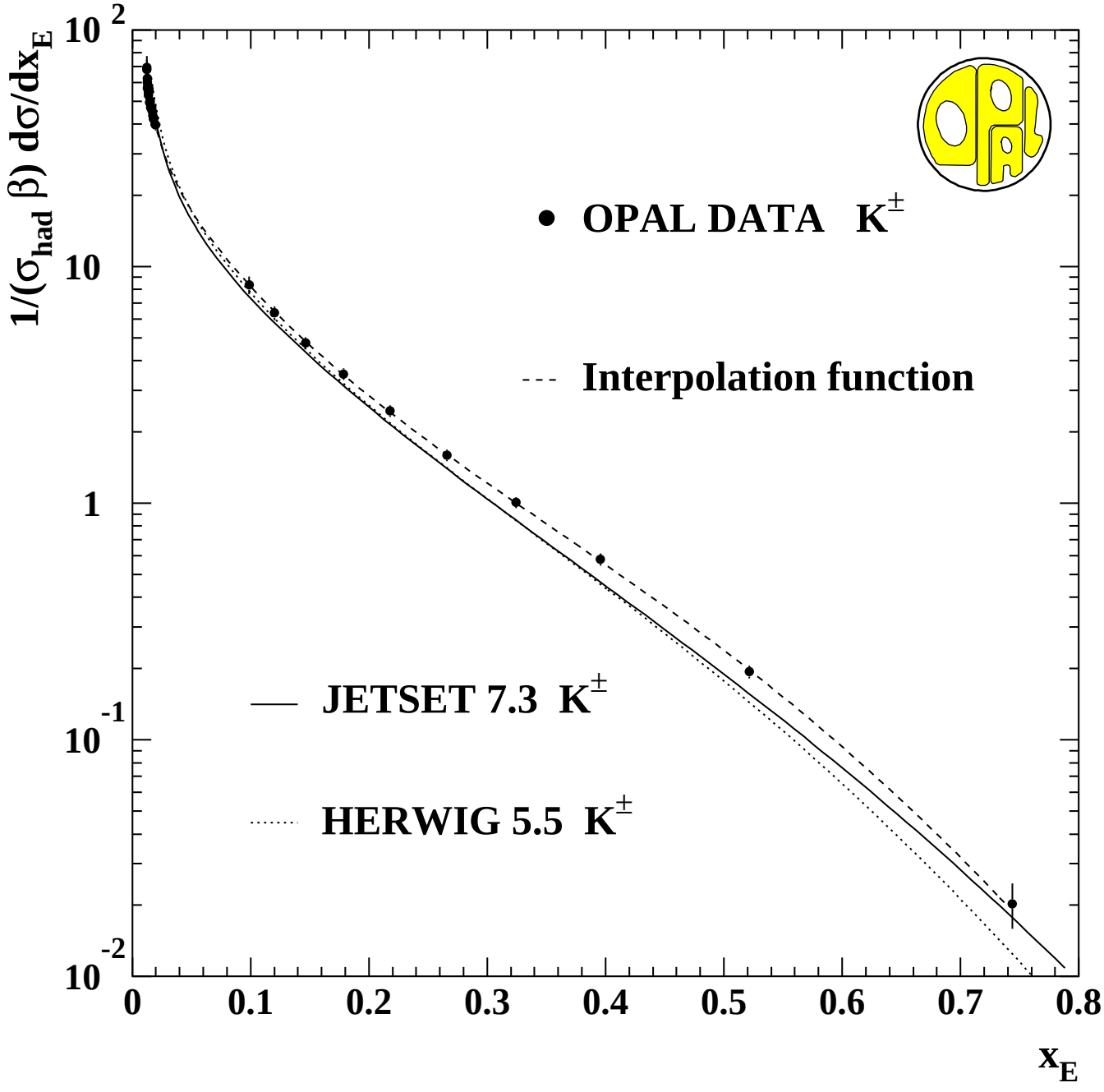
$1/(\sigma_{had}\,\beta)\ d\sigma/dx_E$
10^2
10
1
10^{-1}
10^{-2}
0
0.1
0.2
0.3
0.4
0.5
0.6
0.7
0.8
x_E
OPAL DATA $K^{\pm}$
Interpolation function
JETSET 7.3 $K^{\pm}$
HERWIG 5.5 $K^{\pm}$

Fig. 7c

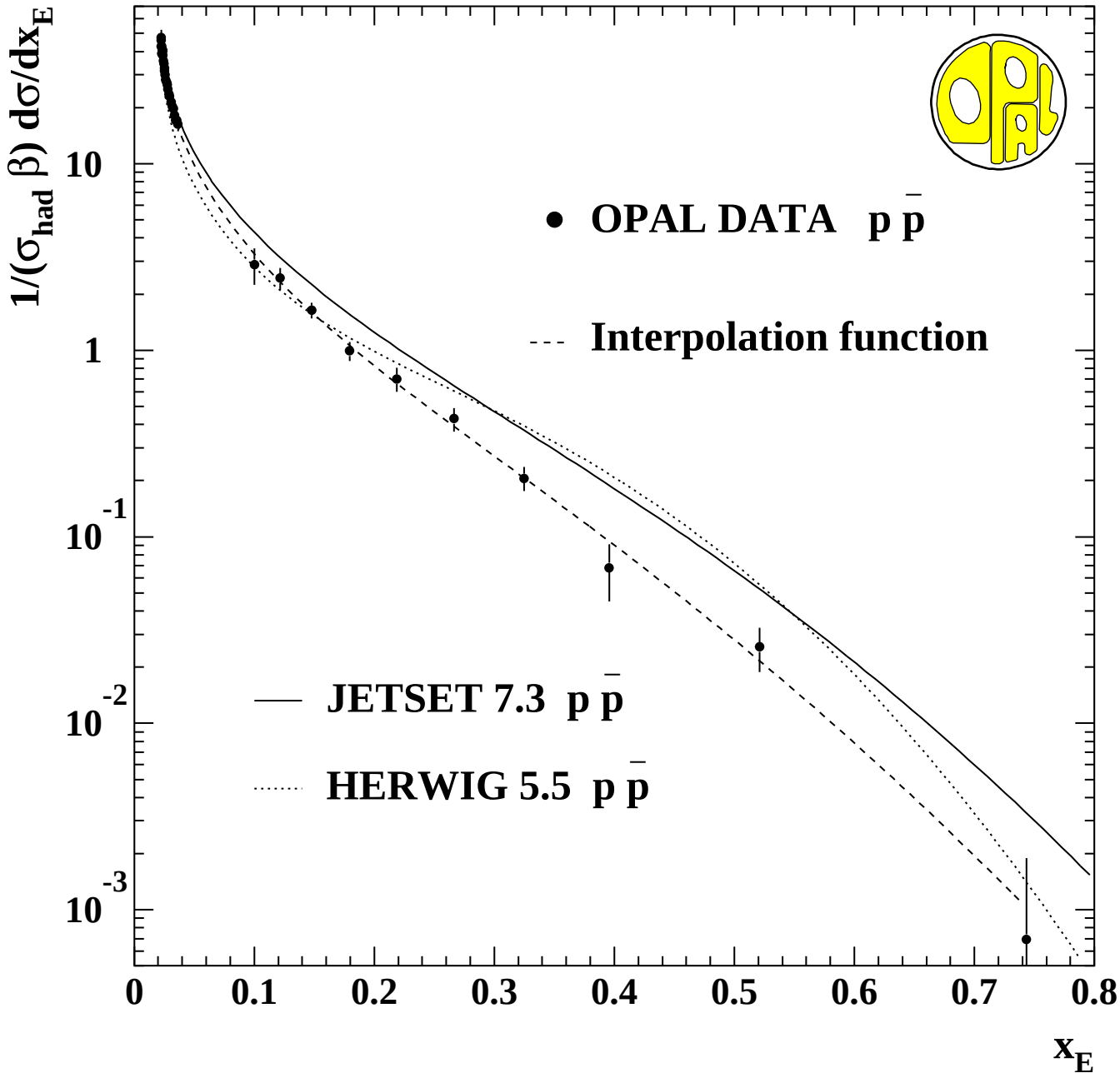
1/(σ_had β) dσ/dx_E
10
1
10^-1
10^-2
10^-3
0
0.1
0.2
0.3
0.4
0.5
0.6
0.7
0.8
x_E
OPAL DATA p p̄
Interpolation function
JETSET 7.3 p p̄
HERWIG 5.5 p p̄

Fig. 8

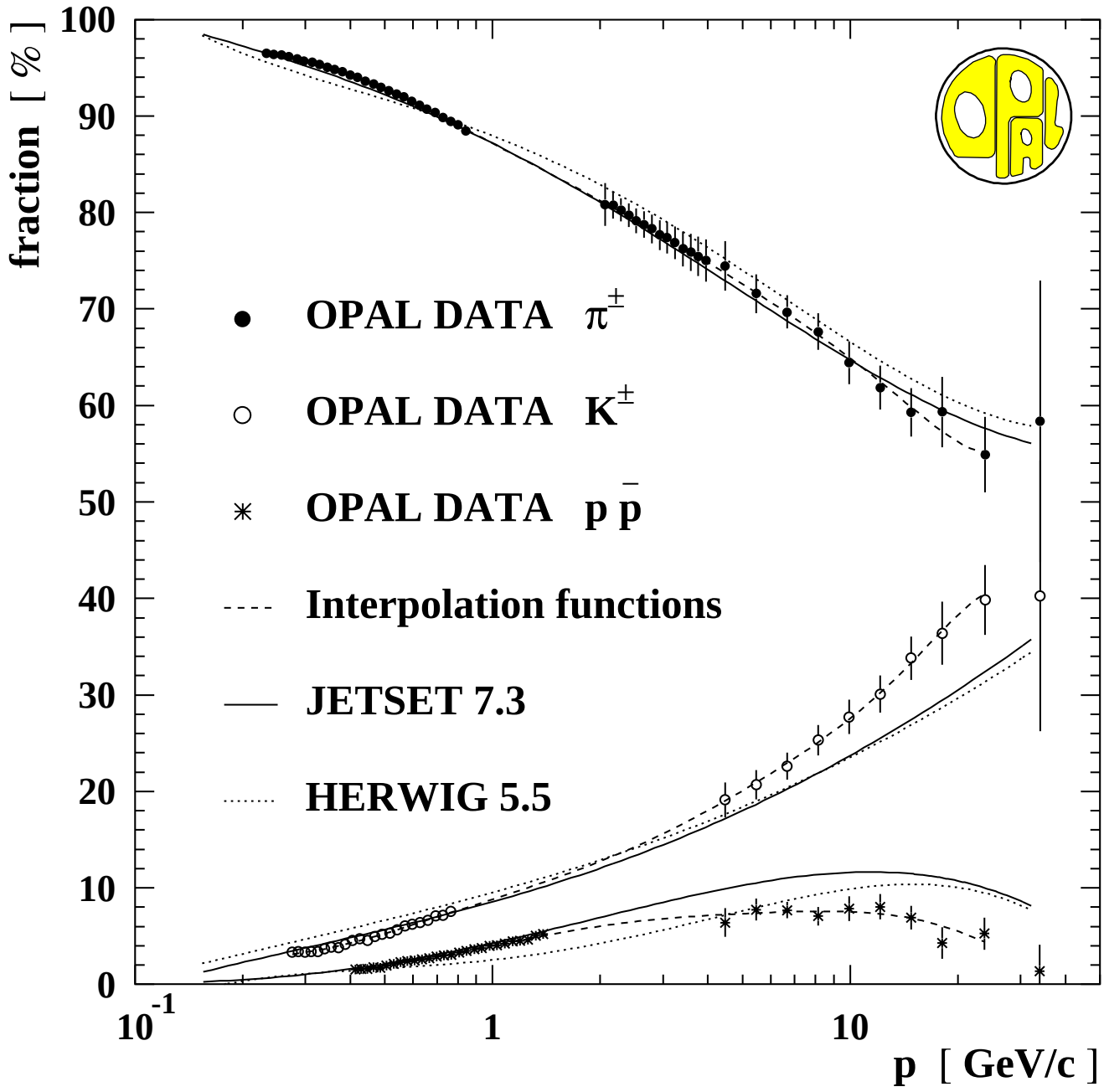
fraction [%]
100
90
80
70
60
50
40
30
20
10
0
10^{-1}
1
10
p [GeV/c]
OPAL DATA $\pi^{\pm}$
OPAL DATA $K^{\pm}$
OPAL DATA $p\bar{p}$
Interpolation functions
JETSET 7.3
HERWIG 5.5

Fig. 9a

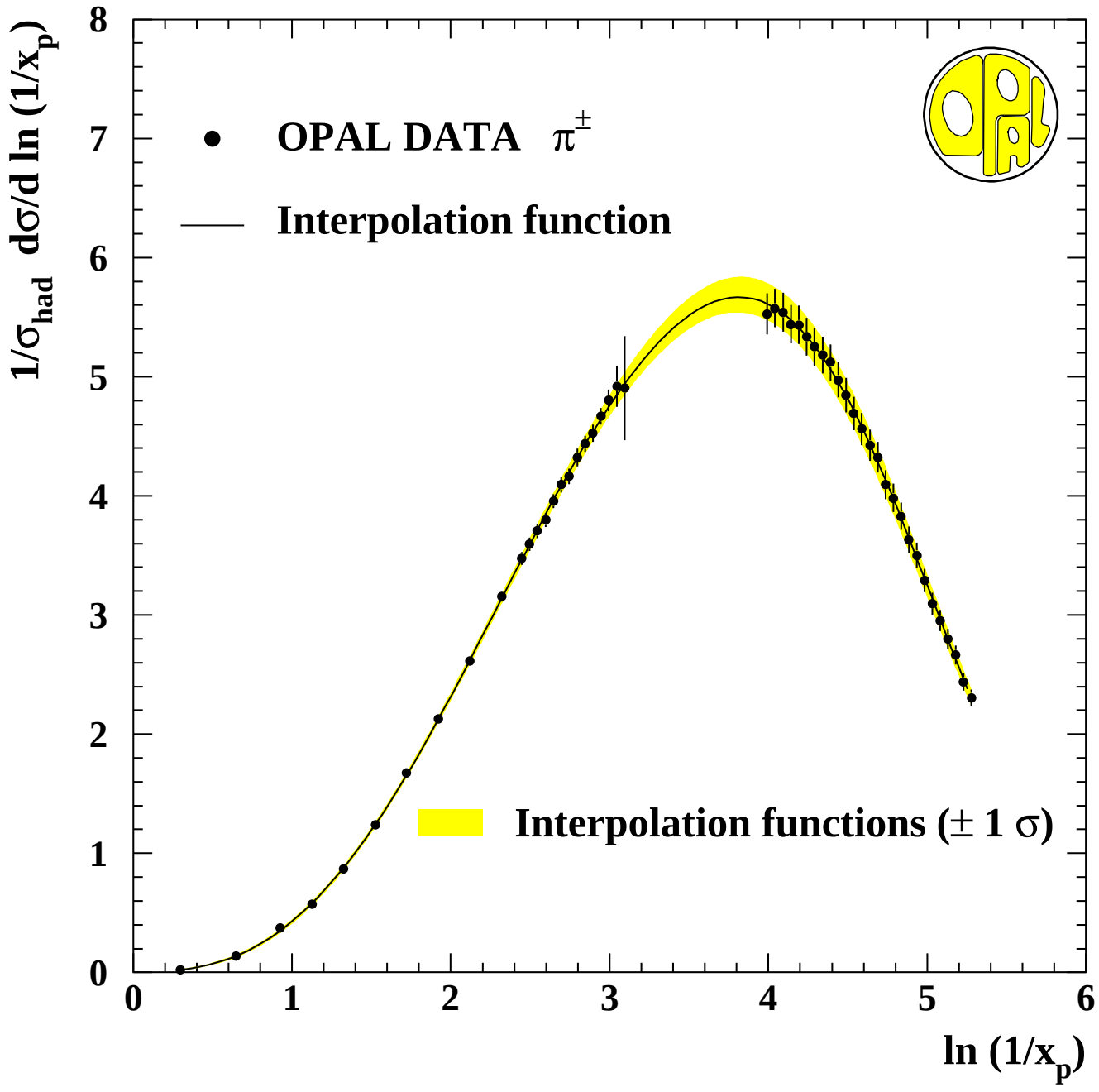
OPAL DATA $\pi^{\pm}$
Interpolation function
Interpolation functions ($\pm$ 1 σ)
$1/\sigma_{had}\ d\sigma/d\ \ln\ (1/x_p)$
$\ln\ (1/x_p)$
0
1
2
3
4
5
6
7
8

Fig. 9b

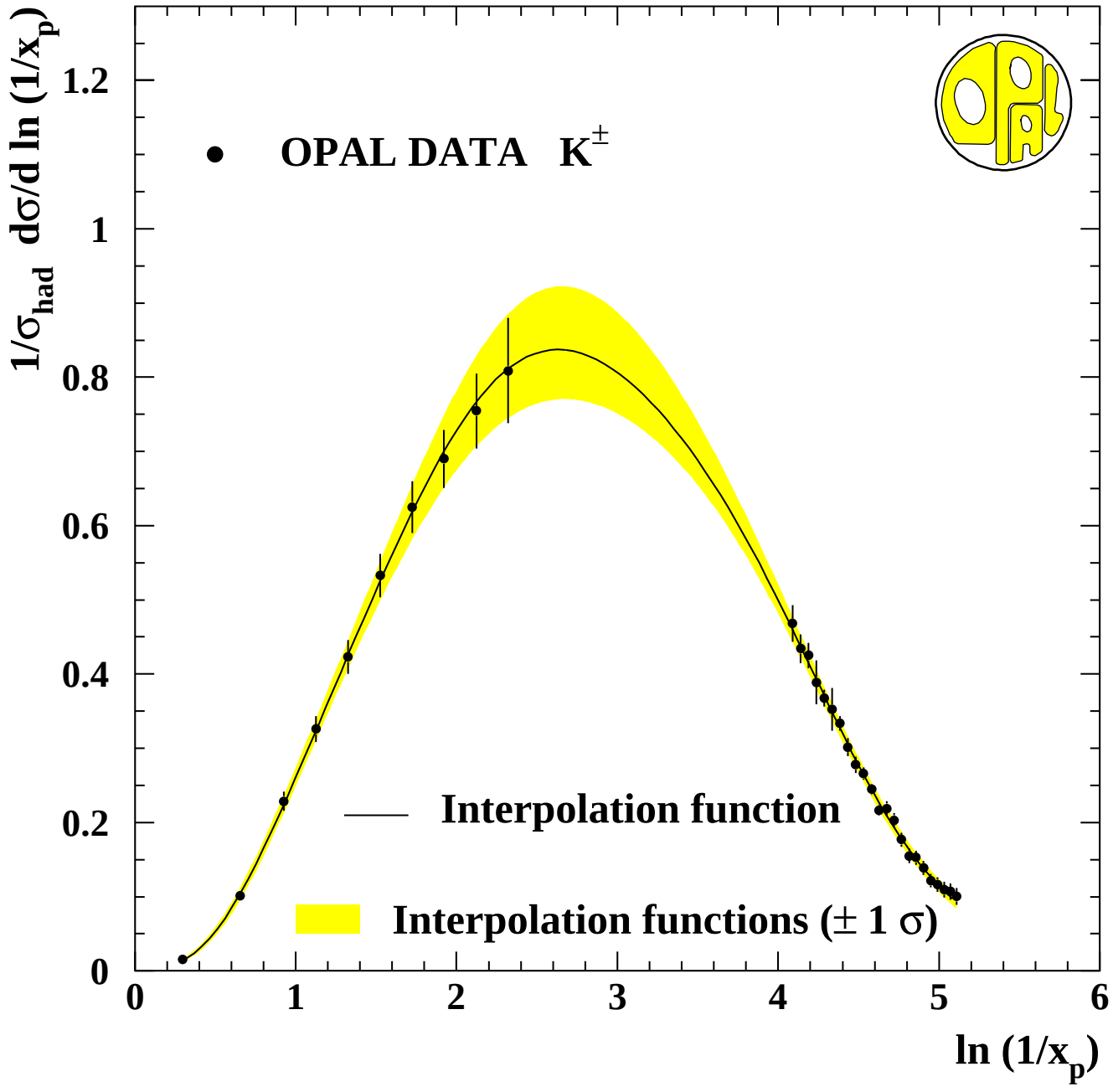
OPAL DATA K±
Interpolation function
Interpolation functions (± 1 σ)
1/σhad dσ/d ln (1/xp)
ln (1/xp)
0
0.2
0.4
0.6
0.8
1
1.2
0
1
2
3
4
5
6

Fig. 9c

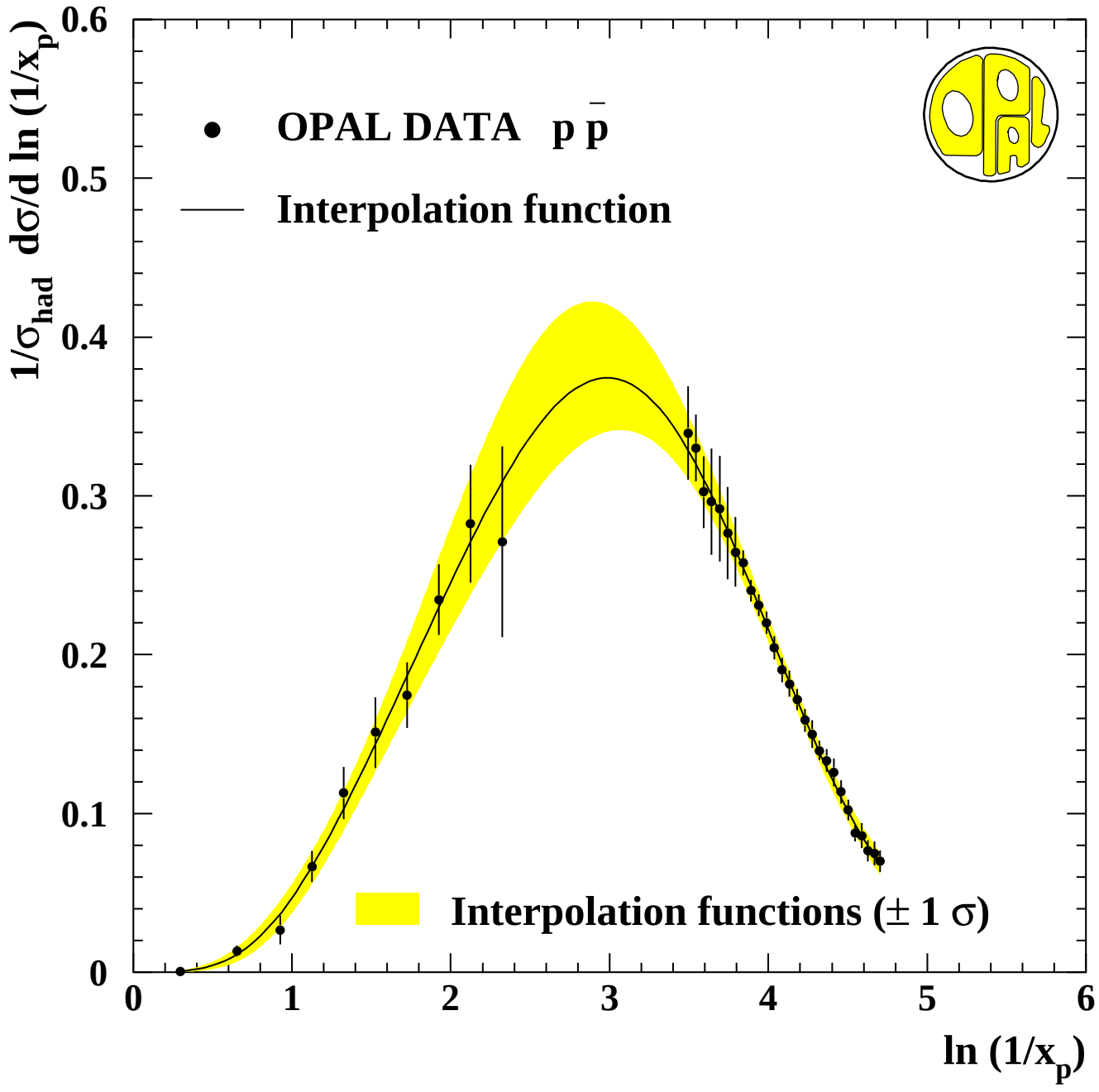
OPAL DATA p p̄
Interpolation function
Interpolation functions (± 1 σ)
1/σ_had dσ/d ln (1/x_p)
ln (1/x_p)
0
0.1
0.2
0.3
0.4
0.5
0.6
0
1
2
3
4
5
6

Fig. 10

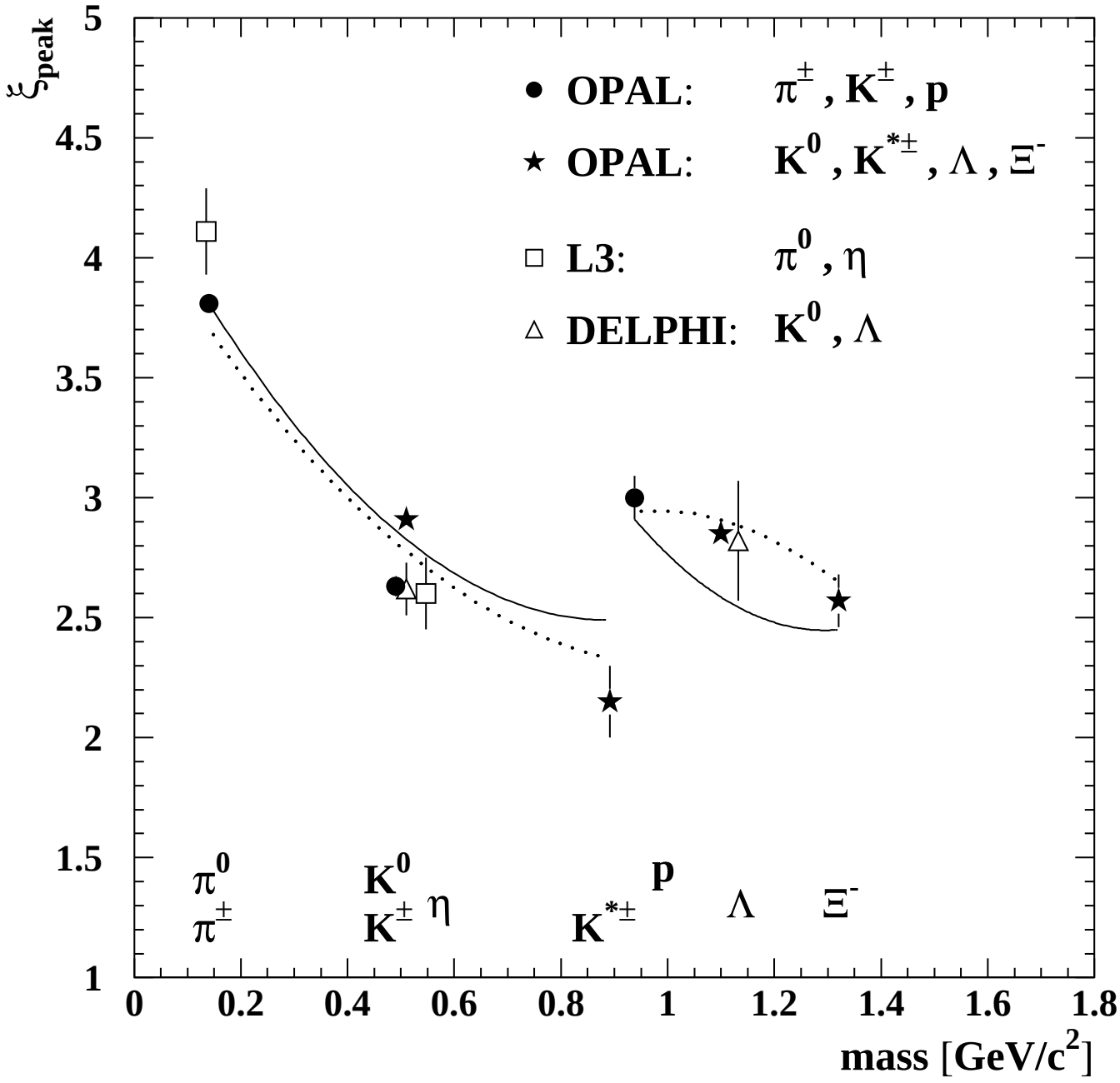
ξ_{peak}
5
4.5
4
3.5
3
2.5
2
1.5
1
0
0.2
0.4
0.6
0.8
1
1.2
1.4
1.6
1.8
mass [GeV/c^2]
OPAL: $\pi^{\pm}$, $K^{\pm}$, p
OPAL: K^0, $K^{*\pm}$, Λ, Ξ^-
L3: π^0, η
DELPHI: K^0, Λ
π^0
$\pi^{\pm}$
K^0
$K^{\pm}$ η
$K^{*\pm}$
p
Λ
Ξ^-